

Gated Linear Attention Transformers with Hardware-Efficient Training

Songlin Yang^{1*}, Bailin Wang^{1*}, Yikang Shen², Rameswar Panda², Yoon Kim¹

¹Massachusetts Institute of Technology

²MIT-IBM Watson AI Lab

{yangsl66, bailinw, yoonkim}@mit.edu
{yikang.shen, rpanda}@ibm.com

Abstract

Transformers with linear attention allow for efficient parallel training but can simultaneously be formulated as an RNN with 2D (matrix-valued) hidden states, thus enjoying linear (with respect to output length) inference complexity. Recent works such as RetNet (Sun et al., 2023) and TransNormerLLM (Qin et al., 2023a) observe that adding a global decay term to the additive RNN update rule greatly improves performance, sometimes outperforming standard Transformers with softmax attention when trained at scale. In this work we show that adding a *data-dependent* gating mechanism further improves performance. We derive a parallel form of this gated linear attention layer that enables efficient training. However, a straightforward, numerically stable implementation of this parallel form requires generalized matrix multiplications in log-space for numerical stability, and thus cannot take advantage of tensor cores on modern GPUs which are optimized for standard matrix multiplications. We develop a hardware-efficient version of the parallel form that can still make use of tensor cores through *block-parallel* computations over sequence chunks. Experiments on moderate-scale language modeling (340M-parameter models trained on 15B tokens, 1.3B-parameter models trained on 100B tokens) show that gated linear attention (GLA) Transformers perform competitively against a strong LLaMA-architecture Transformer baseline (Touvron et al., 2023) as well as Mamba (Gu & Dao, 2023), a recently introduced state-space model with a data-dependent state transition mechanism. For training speed, our Triton-based implementation performs comparably to CUDA-optimized FlashAttention-2 (Dao, 2023) under the regular 2048 training length setting, while outperforming FlashAttention-2 when training on longer sequences beyond ¹.

1 Introduction

Transformers with softmax attention (Vaswani et al., 2017) enjoy efficient parallel training but suffer from quadratic (in sequence length) complexity for both training and inference, thus motivating more RNN-like models that allow for linear-time sequence modeling. Linear attention Transformers, which replace the softmax attention mechanism with a simple dot product over (possibly transformed) key/query vectors, has emerged as a promising alternative to classic softmax attention (Katharopoulos et al., 2020; Choromanski et al., 2020; Kasai et al., 2021b; Peng et al., 2021). An attractive property of linear attention Transformers is that they admit a “recurrent form” in which they can be formulated as an RNN with 2D hidden states that are additively updated at each time step (Katharopoulos et al., 2020). This recurrent form is especially useful since the entire history can be compressed into the matrix-valued hidden state, thus eliminating the need to maintain and attend over a KV cache during inference. For training, linear attention Transformers also admit a sub-quadratic “chunk-wise parallel form” which divides the sequence into non-overlapping chunks and performs (serial) inter-chunk recurrent computations followed by (parallel) intra-chunk computations (Hua et al., 2022; Sun et al., 2023; Lingle, 2023), thus (partially) maintaining parallel training.

*Equal contribution. Order determined by coin flip.

¹Code will be available at <https://github.com/berlino/gated.linear.attention>.

RetNet (Sun et al., 2023) and TransNormerLLM (Qin et al., 2023a) obtain further improvements over linear attention by adding a decay factor to the additive recurrent update. However, to maintain parallel training they use a global, *data-independent* decay factor, despite the fact that in 1D RNNs, a *data-dependent* gating mechanism—in particular, a forget gate that can remove information from the hidden states—has been shown to be crucial for performance (van der Westhuizen & Lasenby, 2018; Qin et al., 2023b). While Mao (2022) proposes a data-dependent gating mechanism in linear attention Transformers, they rely only on the recurrent form, which results in 1) lack of parallelism due to sequential recurrent updates, 2) high I/O cost to store/load the 2D hidden states for each token into GPU global memory, and 3) floating point of operations (FLOPs) that are dominated by memory-bound element-wise operations instead of half-precision matrix multiplications (matmuls). These issues preclude the recurrent form as a viable option for large-scale pretraining, and indeed, Mao (2022) only experiment with small-scale finetuning of pretrained softmax attention Transformers into linear attention Transformers.

In this work, we derive an efficient training strategy for linear attention Transformers with data-dependent forget gates. We first derive a parallel form of our gated linear attention (GLA) layer, similar to the parallel form of softmax attention. With this form, the RNN outputs can be computed in parallel without materializing the 2D hidden states for all tokens. However, this parallel form by itself is not amenable to tensor core accelerations due to some non-standard matrix multiplication operations that are needed for numerical stability. We further develop a *chunk-wise parallel form* of the GLA layer, which strikes a balance between the recurrent form and the parallel form. This approach employs a chunk-level recurrence to sync information between chunks, while using the parallel form for intra-chunk computations. With this form, we can leverage standard half-precision matrix matmuls for most computations, thus enabling efficient training.

On moderate-scale language modeling experiments, where we train models with 340M/1.3B parameters on 15B/100B tokens respectively, we find that the GLA Transformer performs on par with a (1) strong LLaMA-architecture Transformer baseline which makes use of recent recipes (Transformer⁺⁺; Touvron et al., 2023) as well as (2) Mamba (Gu & Dao, 2023), a recent state-space models that uses data-dependent state transition mechanisms. For training efficiency, our Triton-based implementation (Tillet et al., 2019) performs comparably to CUDA-optimized FlashAttention-2 (Dao, 2023) under the regular 2048 training length setting, while outperforming FlashAttention-2 when training on longer sequences beyond 4096.

2 Background

2.1 Linear Attention Transformers

Standard autoregressive Transformers employ a softmax attention mechanism which takes an input sequence $\mathbf{X} \in \mathbb{R}^{L \times d}$ (here L is the length and d is the hidden dimension) and computes the output $\mathbf{O} \in \mathbb{R}^{L \times d}$ via,

$$\mathbf{Q}, \mathbf{K}, \mathbf{V} = \mathbf{XW}_Q, \mathbf{XW}_K, \mathbf{XW}_V, \quad \mathbf{O} = \text{softmax}((\mathbf{QK}^\top) \odot \mathbf{M})\mathbf{V}, \quad (1)$$

where $\mathbf{W}_Q, \mathbf{W}_K, \mathbf{W}_V \in \mathbb{R}^{d \times d}$ are learnable matrices and $\mathbf{M} \in \{-\infty, 1\}^{L \times L}$ is a mask that prevents the model from attending to future tokens, i.e., $\mathbf{M}_{ij} = 1$ if $i \geq j$ and $\mathbf{M}_{ij} = -\infty$ if $i < j$. (Here we assume a single attention head for simplicity.) The output \mathbf{O} is then passed through a series of feedforward layers along with residual connections and layer normalization to obtain the next layer’s representation.

The above *parallel form* of attention can compute \mathbf{O} in parallel given the full input \mathbf{X} , thus enabling efficient GPU training. However, during inference Transformers must use the following *iterative form*,

$$\mathbf{Q}_t, \mathbf{K}_t, \mathbf{V}_t = \mathbf{X}_t \mathbf{W}_Q, \mathbf{X}_t \mathbf{W}_K, \mathbf{X}_t \mathbf{W}_V, \quad \mathbf{O}_t = \frac{\sum_{i=1}^t \exp(\mathbf{Q}_t \mathbf{K}_i^\top) \mathbf{V}_i}{\sum_{i=1}^t \exp(\mathbf{Q}_t \mathbf{K}_i^\top)},$$

which calculates the query (\mathbf{Q}_t), key (\mathbf{K}_t), and value (\mathbf{V}_t) vectors given the current token’s representation $\mathbf{X}_t \in \mathbb{R}^{1 \times d}$ and the performs attention over the set of keys $\{\mathbf{K}_1, \dots, \mathbf{K}_t\}$ and values $\{\mathbf{V}_1, \dots, \mathbf{V}_t\}$ (i.e., the “KV cache”), both of which grow over time.

Linear attention mechanisms (Katharopoulos et al., 2020) replace $\exp(\mathbf{Q}_t \mathbf{K}_i^\top)$ with a kernel $k(\mathbf{x}, \mathbf{y})$ with an associated feature map ϕ (i.e., $k(\mathbf{x}, \mathbf{y}) = \langle \phi(\mathbf{x}), \phi(\mathbf{y}) \rangle$). This simplifies the calculation of \mathbf{O}_t since we have

$$\mathbf{O}_t = \frac{\sum_{i=1}^t \phi(\mathbf{Q}_t) \phi(\mathbf{K}_i)^\top \mathbf{V}_i}{\sum_{i=1}^t \phi(\mathbf{Q}_t) \phi(\mathbf{K}_i)^\top} = \frac{\phi(\mathbf{Q}_t) \sum_{i=1}^t \phi(\mathbf{K}_i)^\top \mathbf{V}_i}{\phi(\mathbf{Q}_t) \sum_{i=1}^t \phi(\mathbf{K}_i)^\top}. \quad (2)$$

Letting $\mathbf{S}_t = \sum_{i=1}^t \phi(\mathbf{K}_i)^\top \mathbf{V}_i$ and $\mathbf{z}_t = \sum_{i=1}^t \phi(\mathbf{K}_i)^\top$ where $\mathbf{S}_t \in \mathbb{R}^{d \times d}$, $\mathbf{z}_t \in \mathbb{R}^{d \times 1}$, we can rewrite Eq. 2 as:

$$\mathbf{S}_t = \mathbf{S}_{t-1} + \phi(\mathbf{K}_t)^\top \mathbf{V}_t, \quad \mathbf{z}_t = \mathbf{z}_{t-1} + \phi(\mathbf{K}_t)^\top, \quad \mathbf{O}_t = \frac{\phi(\mathbf{Q}_t) \mathbf{S}_t}{\phi(\mathbf{Q}_t) \mathbf{z}_t}.$$

Although various kernels have been explored (Kasai et al., 2021b; Peng et al., 2021; Choromanski et al., 2020), recent work (Mao, 2022; Sun et al., 2023) has found that a linear kernel (i.e., setting ϕ to be the identity) works well in practice. Qin et al. (2022) further find that the normalizer \mathbf{z}_t can result in instabilities and suggest removing \mathbf{z}_t and instead apply normalization in the output layer. This results in an (unnormalized) linear attention Transformer with the following update equation,

$$\mathbf{S}_t = \mathbf{S}_{t-1} + \mathbf{K}_t^\top \mathbf{V}_t, \quad \mathbf{O}_t = \mathbf{Q}_t \mathbf{S}_t. \quad (3)$$

Eq. 3 makes it clear that a linear attention Transformer is essentially a linear RNN with matrix-valued hidden states \mathbf{S}_t that is updated via the outer-product $\mathbf{K}_t^\top \mathbf{V}_t = (\mathbf{X}_t \mathbf{W}_K)^\top (\mathbf{X}_t \mathbf{W}_V)$.²

Training efficiency. As is the case with RNNs, linear attention Transformers enjoy linear complexity in both time and memory with respect to the input length L . However in practice this form cannot straightforwardly be used for efficient training since it is not parallelizable (across the temporal dimension). The parallel form of linear attention, whose complexity is (still) quadratic in L , is given by,

$$\mathbf{O} = ((\mathbf{Q} \mathbf{K}^\top) \odot \mathbf{M}) \mathbf{V},$$

where $\mathbf{M} \in \{0, 1\}^{L \times L}$ is a mask such that $\mathbf{M}_{ij} = 1$ if $i \geq j$ and $\mathbf{M}_{ij} = 0$ if $i < j$. The presence of the mask \mathbf{M} means that it is not possible to exploit the associative property of matrix multiplication to reduce the parallel form complexity from quadratic to linear,³ which makes this approach difficult to scale to long contexts. This motivates the hybrid chunk-wise *block-parallel* strategy below.

Chunk-wise block-parallel attention. The block-parallel form strikes a balance between the FLOPs savings from the linear-complexity recurrent form and the parallelizability of the quadratic-complexity parallel form (Hua et al., 2022). This approach minimizes the number of recurrent computations by only performing recurrence at the *chunk-level*, while the computations within a chunk can be computed in parallel using half-precision matmuls without explicitly materializing the hidden states. Conceptually, this consists of two steps: *inter-chunk recurrence* to propagate the hidden states at chunk-level, followed by *intra-chunk parallel computation* in parallel form to directly compute the output \mathbf{O} based on the chunk-level hidden states.

More formally, suppose the input \mathbf{X} is now split into non-overlapping chunks, where each chunk is of length C . Following the notation from Sun et al. (2023), let $\mathbf{S}_{[i]} \in \mathbb{R}^{d \times d}$ be the chunk-level hidden state after processing i chunks, i.e., $\mathbf{S}_{[i]} := \mathbf{S}_{iC}$. Further let $\mathbf{Q}_{[i]} := \mathbf{Q}_{iC+1:(i+1)C} \in \mathbb{R}^{C \times d}$ be the query vectors corresponding to the i -th chunk; $\mathbf{K}_{[i]}$, $\mathbf{V}_{[i]}$, $\mathbf{O}_{[i]}$ are similarly defined. We then have (for $i \in [0, 1, \dots, \frac{L}{C} - 1]$):

1. Inter-chunk recurrence:

$$\mathbf{S}_{[i+1]} = \mathbf{S}_{[i]} + \underbrace{\sum_{j=iC+1}^{(i+1)C} \mathbf{K}_{[i]}^\top \mathbf{V}_{[j]}}_{\mathbf{K}_{[i]}^\top \mathbf{V}_{[i]}} \in \mathbb{R}^{d \times d}. \quad (4)$$

Here $\mathbf{S}_{[0]}$ is initialized to the zero,⁴ and the sum of all RNN inputs from a chunk (i.e., $\mathbf{K}_{[i]}^\top \mathbf{V}_{[i]}$) can be computed *before* the recurrence in parallel in $O(C^2 d)$.

²This type of model with matrix-valued hidden states that change over time is also known as “fast weights” (Hinton & Plaut, 1987; Schmidhuber, 1992; Ba et al., 2016), which was recently explored in the context of linear Transformers (Schlag et al., 2021; Irie et al., 2021; Mao, 2022).

³Without \mathbf{M} , one can transform $(\mathbf{Q} \mathbf{K}^\top) \mathbf{V}$ to $\mathbf{Q}(\mathbf{K}^\top \mathbf{V})$ reducing the complexity from quadratic ($O(L^2 d)$) to linear ($O(L d^2)$).

⁴It is possible to initialize this with historical states, as is commonly done when training 1D RNNs.

2. Intra-chunk parallel computation:

$$\mathbf{O}_{[i+1]} = \underbrace{\mathbf{Q}_{[i+1]} \mathbf{S}_{[i]}}_{\text{cross-chunk}} + \underbrace{((\mathbf{Q}_{[i+1]} \mathbf{K}_{[i+1]}^\top) \odot \mathbf{M}) \mathbf{V}_{[i+1]}}_{\text{intra-chunk}} \in \mathbb{R}^{C \times d}. \quad (5)$$

Here the “intra-chunk” component has exactly the same parallel form as Eq. 3 and thus takes $O(C^2d + Cd^2)$, while the “cross-chunk” component accounts for the contribution from the hidden state from the previous chunk, and takes $O(Cd^2)$.

Computation proceeds by first obtaining $\mathbf{S}_{[1]}, \dots, \mathbf{S}_{[\frac{L}{C}]}$ with the inter-chunk recurrence computations. Once these have been computed, the intra-chunk computation can be performed in parallel. Training complexity is thus $O\left(\frac{L}{C}(C^2d + Cd^2)\right) = O(LCd + Ld^2)$, which is less than $O(L^2d)$ when $L > d$. The choice of C relies on a trade-off between FLOPs and wall-clock speed: larger chunk sizes result in more FLOPs due to the intra-chunk parallel computation; smaller C results in fewer FLOPs, but also requires more recurrent (non-parallelizable) computations, leading to slower wall-clock speeds.

2.2 Linear Attention with Decay: RetNet and TransNormerLLM

Eq. 3 indicates that the simplified linear Transformer is an RNN where the hidden states are 2D arrays (i.e., matrices) instead of 1D arrays. Gating mechanism which allow an RNN to “forget” have proved crucial for conventional 1D RNNs (van der Westhuizen & Lasenby, 2018; Qin et al., 2023b). Similarly, recent variants of linear attention Transformers, in particular RetNet (Sun et al., 2023) and TransNormerLLM (Qin et al., 2023a), introduce a forgetting mechanism via a *fixed* decay factor $\gamma \in (0, 1)$ ⁵

$$\mathbf{S}_t = \gamma \mathbf{S}_{t-1} + \mathbf{K}_t^\top \mathbf{V}_t. \quad (6)$$

This can be easily incorporated into the parallel form of attention,

$$\mathbf{O} = (\mathbf{Q} \mathbf{K}^\top \odot \mathbf{D}) \mathbf{V}, \quad \mathbf{D}_{nm} = \begin{cases} \gamma^{n-m}, & n \geq m \\ 0, & n < m \end{cases}. \quad (7)$$

The block-parallel form of this linear attention with decay has the inter-chunk recurrence given by,

$$\begin{aligned} \mathbf{S}_{[i+1]} &= \gamma^C \mathbf{S}_{[i]} + \sum_{j=iC+1}^{(i+1)C} \gamma^{(i+1)C-j} \mathbf{K}_j^\top \mathbf{V}_j \\ &= \gamma^C \mathbf{S}_{[i]} + \mathbf{K}_{[i+1]}^\top (\mathbf{V}_{[i+1]} \odot \Gamma), \end{aligned}$$

where we have $\Gamma_{ij} = \gamma^{C-i}$ for all j . The intra-chunk parallel computation is then given by,

$$\mathbf{O}_{[i+1]} = \underbrace{(\mathbf{Q}_{[i+1]} \mathbf{S}_{[i]} \odot \Lambda)}_{\text{cross-chunk}} + \underbrace{(\mathbf{Q} \mathbf{K}^\top \odot \mathbf{D}) \mathbf{V}}_{\text{intra-chunk}}, \quad \Lambda_{ij} = \gamma^i.$$

Compared with the intra-chunk parallel computation of linear attention in Eq. 5, both the inter- and intra-chunk computations need to account for the decay factor.

2.3 Hardware Considerations for Training Linear Attention Transformers

We re-examine the above three forms (i.e., recurrent, parallel, block-parallel) from the perspective of hardware efficiency. As prerequisite, we briefly provide an overview of GPU characteristics, and refer readers to Fu et al. (2023, Sect. 2.2) and the Appendix for further details. An efficient training algorithm needs to be aware of the compute model, memory hierarchy and specialized compute units in GPUs. In particular:

⁵In practice these works adopt a complex-valued decay factor, but for simplicity of discussion here we only consider the magnitude part of the complex-valued decay factor, which has can be seen as an exponential decay. The phase part performs a similar role to the Rotary Position Embedding (RoPE; Su et al., 2021).

- GPUs have many threads executed in parallel; threads are grouped into thread blocks, which execute on Streaming Multiprocessors (SMs). An A100, for example, has 108 SMs. To maintain a high GPU occupancy (i.e., fraction of GPU resources being used), it is necessary to use a sufficient number of SMs.
- GPUs have a memory hierarchy with larger but slower global GPU memory (high bandwidth memory; HBM) and smaller but faster shared memory (SRAM). Optimal utilization of SRAM to reduce HBM I/O cost can therefore lead to significant speed-ups; for example, the attention mechanism is memory-bound and benefits significantly from recomputation, tiling, and kernel fusion, as demonstrated in FlashAttention-1 (Dao et al., 2022).
- GPUs have specific computation units, i.e., *tensor cores*, to accelerate half-precision matmuls with much higher FLOP/s than other general-purposed operations. For example, half-precision matmuls on an A100 can be roughly 16 times faster, and recent works such as FlashAttention-2 (Dao, 2023) and FlashConvFFT (Fu et al., 2023) aim to minimize FLOPs in non-half-precision matmul operations as much as possible.

We next explain concretely how these considerations are related to training linear attention Transformers.

SM occupancy considerations. In large-scale training and long-sequence modeling scenarios, parallelizing over batch size and number of heads is not sufficient to fully exploit SMs, and it is often necessary to parallelize over the temporal dimension for high GPU occupancy (Dao, 2023). The parallel form and the block-parallel form can parallelize along the temporal dimension in addition to batch size and number of heads, which results in better utilization of GPU multiprocessors. The recurrent form lacks such parallelism, generally resulting in much lower GPU occupancy.⁶

Computation considerations. In general the recurrent form has the lowest FLOPs.⁷ However, it does not involve any matmuls and thus cannot leverage tensor cores. The parallel form has the largest number of FLOPs but can leverage tensor cores for acceleration. The block-parallel form has a moderate number of FLOPs and can be accelerated by tensor cores for *most* operations. The only operation that disallows tensor core is the inter-chunk recurrent update part, which is lightweight (i.e., linear element-wise recurrence) and fairly fast in practice with kernel fusion.

Memory considerations. Memory operations involving HBM are expensive. A direct implementation of the recurrent form requires storing 2D hidden states in HBM for gradient estimation, resulting in high I/O cost. Katharopoulos et al. (2020, Sect. 3.3.1) give a two-pass algorithm for gradient computation that avoids such materialization in HBM. As such, the recurrent form can be memory-efficient during training. The parallel form needs to materialize the $O(L^2)$ “attention matrix” into HBM, which can be expensive for long sequences. However, it is possible to use the recomputation technique from FlashAttention (Dao et al., 2022) to avoid such materialization, as was employed in TransNormerLLM (Qin et al., 2023a). For the block-parallel form, one needs to materialize a 2D hidden state into HBM for each chunk. Hence the I/O cost is related to the number of chunks and thus it is important to carefully choose a chunk size in order to strike an optimal balance between total FLOPs and I/O cost (Hua et al., 2022).

3 Gated Linear Attention Transformers

The decay factor in the RetNet update rule (Eq. 6) means that inputs that are more recent are given greater weight, which is arguably reasonable for many applications of interest. However, this decay factor is data-independent, and such a coarse gating mechanism is unlikely to be optimal, even though it does enable straightforward parallel and block-parallel forms. Indeed, in 1D RNNs data-dependent gating mechanisms are

⁶The recurrent form could split the value matrix into several blocks, distributed in different SMs for execution to improve SM occupancy, as implemented in Katharopoulos et al. (2020). Still, the lack of parallelism in the temporal dimension is a fundamental limitation, especially in the setting of large-scale training and long-sequence modeling, wherein the product of batch size and number of heads is small thus SMs are not fully exploited.

⁷The sequence length is generally larger than the head dimension.

generally considered standard for practical sequence modeling (Hochreiter & Schmidhuber, 1997; Cho et al., 2014). In this work we similarly explore an data-dependent gating mechanism for linear attention Transformers, and develop a practical parallel and block-parallel form of attention that can take advantage of tensor core computations on modern GPUs for efficient training.

3.1 Recurrent Form

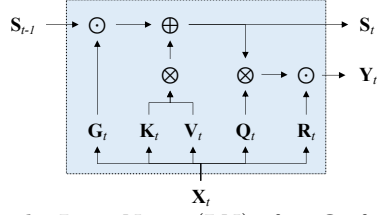
We first present the recurrent formulation of the gated linear attention (GLA) layer. Given an input $\mathbf{X} \in \mathbb{R}^{L \times d}$, we obtain the query/key/value vectors as follows,

$$\mathbf{Q} = \mathbf{X} \mathbf{W}_Q \in \mathbb{R}^{L \times d_k}, \quad \mathbf{K} = \mathbf{X} \mathbf{W}_K \in \mathbb{R}^{L \times d_k}, \quad \mathbf{V} = \mathbf{X} \mathbf{W}_V \in \mathbb{R}^{L \times d_v},$$

where we now allow for different number of dimensions for these vectors. To update the hidden states, we first compute a gating matrix \mathbf{G} given by an outer-product (similar to Mao (2022) and Pramanik et al. (2023)),

$$\mathbf{G}_t = \boldsymbol{\alpha}^\top \boldsymbol{\beta}_t \in \mathbb{R}^{d_k \times d_v}, \quad \boldsymbol{\alpha} = \sigma(\mathbf{X} \mathbf{W}_\alpha + \mathbf{b}_\alpha) / \tau \in \mathbb{R}^{L \times d_k}, \quad \boldsymbol{\beta} = \sigma(\mathbf{X} \mathbf{W}_\beta + \mathbf{b}_\beta) / \tau \in \mathbb{R}^{L \times d_v},$$

where σ is the Sigmoid function and $\tau \in \mathbb{R}$ is a temperature term.⁸ This outer-product-based parameterization of \mathbf{G}_t is parameter-efficient⁹ and it moreover has the same outer-product structure as the RNN input $\mathbf{K}_t^\top \mathbf{V}_t$ which, as we will shortly see, allow for equivalent parallel forms. The output of a GLA layer for time step t is



$$\mathbf{S}_t = \mathbf{G}_t \odot \mathbf{S}_{t-1} + \mathbf{K}_t^\top \mathbf{V}_t \in \mathbb{R}^{d_k \times d_v}, \quad (8)$$

$$\mathbf{Q}_t = \mathbf{Q}_t^\top \mathbf{S}_t \in \mathbb{R}^{1 \times d_v}, \quad (9)$$

$$\mathbf{R}_t = \text{Swish}(\mathbf{X}_t \mathbf{W}_r + \mathbf{b}_r) \in \mathbb{R}^{1 \times d_v}, \quad (10)$$

$$\mathbf{Y}_t = (\mathbf{R}_t \odot \text{LN}(\mathbf{O}_t)) \mathbf{W}_O \in \mathbb{R}^{1 \times d}. \quad (11)$$

The LayerNorm (LN) after \mathbf{O}_t follows prior work which found it to be useful for numerical stability (Qin et al., 2022; 2023a; Sun et al., 2023). The final output \mathbf{Y}_t is obtained by following the structure of a gated attention unit layer (Hua et al., 2022) where an additional output gate \mathbf{R}_t with the Swish activation (Ramachandran et al., 2017) is used; this was also used in RetNet (Sun et al., 2023) and recent state-space models (Mehta et al., 2023; Wang et al., 2022). We also illustrate the recurrent form in the left figure.

Training (in)efficiency of the recurrent form. Mao (2022) also demonstrate the benefit of using a fine-grained gating mechanisms as opposed to a coarse-grained gating mechanism where all elements share a single data-dependent decay term (e.g., as in Peng et al. (2021)). However, their training, which relies on the recurrent form, does not scale well to long context lengths (L) and large hidden dimensions (d_k, d_v), due to the recurrent form’s lack of parallelism and the need to materialize all the hidden states.¹⁰ In particular, the sequential nature of the recurrent form precludes parallelization, and moreover, materializing all the hidden states $\mathbf{S} \in \mathbb{R}^{L \times d_k \times d_v}$ (which is required for gradient computation during the backward pass) makes I/O memory management challenging, even with recomputation techniques.¹¹ While customized CUDA kernels for the recurrent form have been proposed (Katharopoulos et al., 2020; Mao, 2022), they do not bypass these inherent properties of the recurrent form. Potentially due to these limitations, Mao (2022) only experiment with small-scale finetuning of a pretrained softmax attention Transformer (GPT-2) into a gated linear attention Transformer.

⁸Incorporating $\tau > 1$ is to mitigate against the sigmoid outputs quickly saturating. In our experiments, we apply the temperature in log-space: $\log \boldsymbol{\alpha} = (\log \sigma(\mathbf{X} \mathbf{W}_\alpha + \mathbf{b}_\alpha)) / 16$, $\log \boldsymbol{\beta} = (\log \sigma(\mathbf{X} \mathbf{W}_\beta + \mathbf{b}_\beta)) / 16$.

⁹Since it only requires $O(d \times d_k + d \times d_v)$ parameters, while a full parameterization would need $O(d \times d_k \times d_v)$.

¹⁰Mao (2022, Sect. 3.1) claim that gated linear attention transformers cannot employ Katharopoulos et al. (2020, Algorithm 1) to avoid materialization because the gradients w.r.t. data-dependent decay terms depend on the hidden states. In Katharopoulos et al. (2020) there is no learnable decay at all, so there is no need to store hidden states into HBM as other gradient computations do not depend on the hidden states.

¹¹However Pramanik et al. (2023, Sect. 4) recently propose an *approximate* method for estimating the gradient without full materialization, which is orthogonal to our *exact* approach to avoid full materialization.

3.2 Parallel Form

Our core contribution is to develop an efficient and practical parallel form of the gated linear attention layer. We provide a sketch of the derivation below, and defer the full derivation to Appendix B.1. First, we unfold Eq. 8 via,

$$\mathbf{S}_t = \sum_{i=1}^t \left(\left(\prod_{j=i+1}^t \mathbf{G}_j \right) \odot \left(\mathbf{K}_i^\top \mathbf{V}_i \right) \right) \in \mathbb{R}^{d_k \times d_v}.$$

By the mixed product property of Kronecker/outer products, we have

$$\mathbf{G}_t \odot \mathbf{G}_{t+1} = (\boldsymbol{\alpha}_t^\top \boldsymbol{\beta}_t) \odot (\boldsymbol{\alpha}_{t+1}^\top \boldsymbol{\beta}_{t+1}) = (\boldsymbol{\alpha}_t \odot \boldsymbol{\alpha}_{t+1})^\top (\boldsymbol{\beta}_t \odot \boldsymbol{\beta}_{t+1}) \in \mathbb{R}^{d_k \times d_v}.$$

Therefore by induction we further have

$$\prod_{j=i+1}^t \mathbf{G}_j = \left(\prod_{j=i+1}^t \boldsymbol{\alpha}_j \right)^\top \left(\prod_{j=i+1}^t \boldsymbol{\beta}_j \right) = \left(\frac{\prod_{j=1}^t \boldsymbol{\alpha}_j}{\prod_{j=1}^i \boldsymbol{\alpha}_j} \right)^\top \left(\frac{\prod_{j=1}^t \boldsymbol{\beta}_j}{\prod_{j=1}^i \boldsymbol{\beta}_j} \right) = \left(\frac{\mathbf{A}_t}{\mathbf{A}_i} \right)^\top \left(\frac{\mathbf{B}_t}{\mathbf{B}_i} \right)$$

where we have defined $\mathbf{A}_t := \prod_{j=1}^t \boldsymbol{\alpha}_j \in \mathbb{R}^{1 \times d_k}$ and $\mathbf{B}_t := \prod_{j=1}^t \mathbf{B}_j \in \mathbb{R}^{1 \times d_v}$. (All products and divisions are elementwise.) Putting it together we have,

$$\mathbf{O}_t = \mathbf{Q}_t \mathbf{S}_t = \sum_{i=1}^t \left((\mathbf{Q}_t \odot \mathbf{A}_t) \left(\frac{\mathbf{K}_i}{\mathbf{A}_i} \right)^\top \left(\frac{\mathbf{V}_i}{\mathbf{B}_i} \right) \right) \odot \mathbf{B}_t \in \mathbb{R}^{1 \times d_v}.$$

The above form admits the following equivalent parallel form, which can calculate \mathbf{O}_t for all t in parallel,

$$\tilde{\mathbf{Q}} = \mathbf{Q} \odot \mathbf{A}, \quad \tilde{\mathbf{K}} = \mathbf{K}/\mathbf{A}, \quad \tilde{\mathbf{V}} = \mathbf{V}/\mathbf{B}, \quad (12)$$

$$\tilde{\mathbf{O}} = (\tilde{\mathbf{Q}} \tilde{\mathbf{K}}^\top \odot \mathbf{M}) \tilde{\mathbf{V}}, \quad \mathbf{O} = \tilde{\mathbf{O}} \odot \mathbf{B}, \quad (13)$$

where $\mathbf{Q}, \mathbf{K}, \mathbf{A} \in \mathbb{R}^{L \times d_k}$, $\mathbf{V}, \mathbf{B} \in \mathbb{R}^{L \times d_v}$, $\mathbf{O} \in \mathbb{R}^{L \times d}$. Here $\mathbf{M} \in \mathbb{R}^{L \times L}$ denotes the causal mask. As was the case in linear attention, the complexity of the parallel form is quadratic with respect to L . However, there is no need to explicitly materialize the hidden states $\mathbf{S} \in \mathbb{R}^{L \times d_k \times d_v}$, making this approach significantly more memory-efficient.¹²

Numerical issues. \mathbf{A}_t and \mathbf{B}_t are cumulative products of outputs of a sigmoid, and thus can be extremely small when t is large, making \mathbf{K}, \mathbf{V} explode. For numerical stability, we can choose to perform Eq. 13 in log-space through a custom CUDA kernel which implements *generalized* matrix multiplications with a newly defined semi-ring (see Appendix B.1 for details). However, this custom CUDA kernel cannot leverage tensor core computations, and in preliminary experiments we found this generalized matmul to be unacceptably slow. We thus seek alternative training algorithms that can use standard matrix multiplication which can make use of tensor core computations.

3.3 Chunk-wise Block-Parallel Form

We now describe the chunk-wise block-parallel form which, as was the case in linear attention, makes the complexity sub-quadratic in L (when $L > d$) and addresses the numerical issue outlined above. We again present a sketch here and defer the full derivation to Appendix B.1.

As before, suppose \mathbf{X} is now split into $\frac{L}{C}$ chunks, each of length C . Let $\mathbf{S}_{[i]} \in \mathbb{R}^{d_k \times d_v}$ be the chunk-level hidden state after processing i chunks, i.e., $\mathbf{S}_{[i]} := \mathbf{S}_{iC}$. Further let $\mathbf{K}_{[i]} := \mathbf{K}_{iC+1:(i+1)C} \in \mathbb{R}^{C \times d_k}$, $\mathbf{V}_{[i]} := \mathbf{V}_{iC+1:(i+1)C} \in \mathbb{R}^{C \times d_v}$, $\mathbf{A}_{[i]} := \mathbf{A}_{iC+1:(i+1)C} \in \mathbb{R}^{C \times d_k}$. The inter-chunk recurrence is then given by,

$$\mathbf{S}_{[i+1]} = \left(\left(\frac{\mathbf{A}_{(i+1)C}}{\mathbf{A}_{iC}} \right)^\top \left(\frac{\mathbf{B}_{(i+1)C}}{\mathbf{B}_{iC}} \right) \right) \odot \mathbf{S}_{[i]} + (\mathbf{A}'_{[i+1]} \odot \mathbf{K}_{[i+1]})^\top (\mathbf{B}'_{[i+1]} \odot \mathbf{V}_{[i+1]}), \quad (14)$$

¹²Concretely, a straightforward implementation would require $O(L \times (d_k + d_v) + L^2)$ memory as opposed to $O(L \times d_k \times d_v)$ memory for hidden states in the recurrent form. It is also possible to make the $O(L^2)$ term to be sub-quadratic by using the recomputation technique from FlashAttention (Dao et al., 2022; Dao, 2023) at the cost of additional FLOPs.

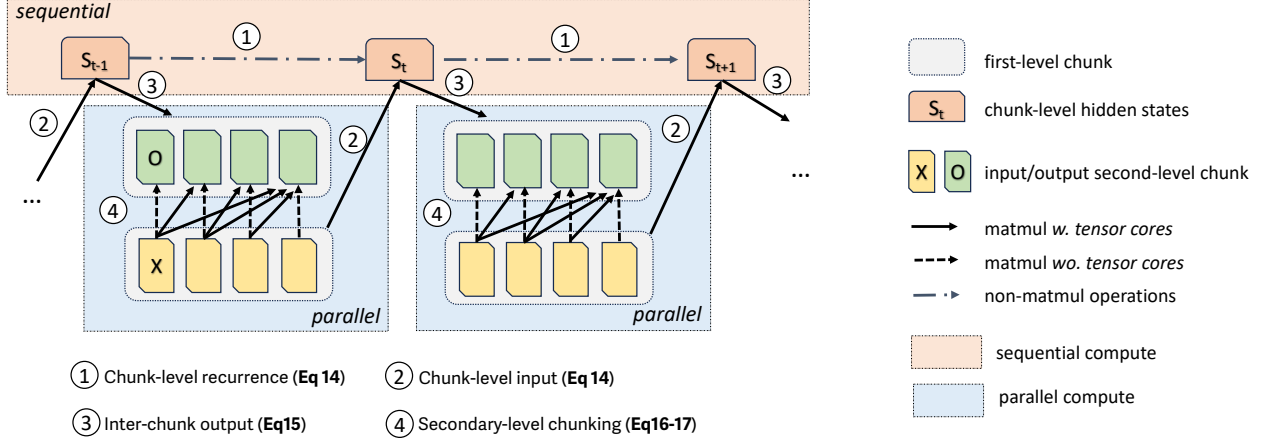


Figure 1: Schematic computation flow of the chunk-wise block-parallel form of the gated linear attention layer. At the first level, we divide a sequence into non-overlapping chunks (grey), and perform intra-chunk computation in parallel while relying on chunk-level (orange) hidden states to sync up information. At the second level, each (yellow) sub-chunk queries all the other sub-chunks within the same chunk in parallel without explicitly materializing the hidden states. The two-level chunking mechanism maximizes the usage of half-precision matmul powered by tensor cores.

where $(\mathbf{A}'_{[i+1]})_j = \frac{\mathbf{A}_{(i+1)C}}{\mathbf{A}_{iC+j}} \in \mathbb{R}^{1 \times d_k}$ and $(\mathbf{B}'_{[i+1]})_j = \frac{\mathbf{B}_{(i+1)C}}{\mathbf{B}_{iC+j}} \in \mathbb{R}^{1 \times d_v}$ for $j \in [1, C]$, $i \in [0, L/C]$. (Therefore we have $\mathbf{A}'_{[i+1]} \in \mathbb{R}^{C \times d_k}$, $\mathbf{B}'_{[i+1]} \in \mathbb{R}^{C \times d_v}$.) The intra-chunk parallel computation is then given by,

$$\tilde{\mathbf{O}}_{[i+1]} = \underbrace{\left((\mathbf{Q}_{[i+1]} \odot \mathbf{A}_{[i+1]}^\dagger) \mathbf{S}_{[i]} \right) \odot \mathbf{B}_{[i+1]}^\dagger}_{\text{cross-chunk}} + \underbrace{(\tilde{\mathbf{Q}}_{[i+1]} \tilde{\mathbf{K}}_{[i+1]}^\top \odot \mathbf{M}) \tilde{\mathbf{V}}_{[i+1]}}_{\text{intra-chunk}}, \quad \mathbf{O}_{[i+1]} = \tilde{\mathbf{O}}_{[i+1]} / \mathbf{B}_{[i+1]}^\dagger, \quad (15)$$

where $(\mathbf{A}_{[i+1]})_j = \frac{\mathbf{A}_{iC+j}}{\mathbf{A}_{iC}} \in \mathbb{R}^{1 \times d_k}$ and $(\mathbf{B}_{[i+1]})_j = \frac{\mathbf{B}_{iC+j}}{\mathbf{B}_{iC}} \in \mathbb{R}^{1 \times d_v}$ for $j \in [1, C]$, $i \in [0, L/C]$. As in Eq. 13, we have $\tilde{\mathbf{Q}}_{[i+1]} = \mathbf{Q}_{[i+1]} \odot \mathbf{A}_{[i+1]}^\dagger$, $\tilde{\mathbf{K}}_{[i+1]} = \frac{\mathbf{K}_{[i+1]}}{\mathbf{A}_{[i+1]}^\dagger}$, $\tilde{\mathbf{V}}_{[i+1]} = \mathbf{V}_{[i+1]} \odot \mathbf{B}_{[i+1]}^\dagger$. For initial values, we set $\mathbf{S}_0 = \mathbf{0}$, $\mathbf{A}_0 = \mathbf{1}$, $\mathbf{B}_0 = \mathbf{1}$. Intuitively, $\mathbf{A}'_{[i]}$ encodes the cumulative decay from the start of a chunk which will be used to propagate the hidden states from the previous chunk $\mathbf{S}_{[i]}$; $\mathbf{A}_{[i]}^\dagger$ encodes the decay to the end of a chunk which will be used to accumulate information to be added to the next hidden state $\mathbf{S}_{[i+1]}$.

The block-parallel form given here is a generalization of the chunk-wise block-parallel forms presented in Section 2. Concretely, if we set $\mathbf{A}_{ij} = 1$, $\mathbf{B}_{ij} = \gamma^{i+1}$, the resulting form becomes RetNet’s chunk-wise form (Sun et al., 2023); if we have $\mathbf{A}_{ij} = 1$ and $\mathbf{B}_{ij} = 1$, we recover the (non-gated) linear attention’s chunk-wise parallel form. As such, our formulation can be regarded as a generalized chunk-wise parallel form for linear attention that enables fine-grained data-controlled decay. This form strikes a balance between the recurrent and the parallel forms in terms of parallelism and numerical stability. Compared with the recurrent form, only the chunk-level hidden states of size $\frac{L}{C} \times d_k \times d_v$ need to be materialized; it is numerically more stable than the parallel form because the sigmoid gates do not need to accumulate beyond a single chunk.

The choice of chunk size C however poses a challenge for further increasing training efficiency. Large chunk size will alleviate the burden of managing chunk-level hidden states, but it will lead to numerical instability (again) due to accumulated multiplications of sigmoids. This motivates the design of secondary-level chunking, where a chunk is further divided into sub-chunks and the interactions between sub-chunks are directly modeled without materializing the hidden states; the pairwise interactions between the sub-chunks can be done via (mostly) half-precision matmuls.

Secondary-level chunking. At a high level, the secondary-level chunking employs an alterative chunk-wise parallel form to the one presented in Eq. 15. It is in the style of self-attention in that it needs to model $O(n^2)$ pair-wise interactions, as opposed to $O(n)$ in the chunk-level recurrence in Eq. 14, where n is the number of

chunks. For simpler notation, we describe this general alternative chunk-wise form below, and in practice we use this at the sub-chunk-level. The key idea is that we can directly model the contribution from i -th chunk to j -th chunk without materializing the 2D hidden states as follows:

$$\mathbf{P}_{[i][j]} = \left(\mathbf{Q}_{[i]} \odot \mathbf{A}_{[i]}^\dagger \right) \left(\mathbf{K}_{[j]} \odot \mathbf{A}'_{[j]} \odot \frac{\mathbf{A}_{iC}}{\mathbf{A}_{(j+1)C}} \right)^\top, \quad (16)$$

$$\mathbf{O}_{[i][j]} = \left(\mathbf{P}_{[i][j]} (\mathbf{V}_{[j]} \odot \mathbf{B}'_{[j]}) \right) \odot \left(\mathbf{B}_{[i]}^\dagger \odot \frac{\mathbf{B}_{iC}}{\mathbf{B}_{(j+1)C}} \right), \quad (17)$$

where $\mathbf{A}', \mathbf{A}^\dagger, \mathbf{B}', \mathbf{B}^\dagger$ are defined as in Eq. 14 and Eq. 15, and we slightly abuse notation and perform broadcasting (when necessary) before the elementwise product \odot . The matrix $\mathbf{P}_{[i][j]} \in \mathbb{R}^{C \times C}$ can be interpreted as the “attention scores” from the i -th chunk to the j -th chunk, and thus $\mathbf{O}_{[i][j]} \in \mathbb{R}^{1 \times d_v}$ is the contribution to $\mathbf{O}_{[j]}$ from the i -th chunk.¹³ The pairwise computation does come at the cost of the more FLOPs than the chunk-level recurrence in Eq. 14, but the memory saving and greater utilization of standard matmuls outweighs the additional FLOP cost, hence contributing to better wall-clock speeds. Specifically, both Eq. 16 and Eq. 17 can be computed efficiently via matmuls. In practice, we choose full-precision matmul when $i = j$, and half-precision matmul when $i < j$, as illustrated in Figure 1.¹⁴

Summary and Discussion. To summarize, we propose a two-level chunking algorithm based on a new chunk-wise block-parallel form which strikes a balance between the recurrent form and the parallel form in terms of parallelism and numerical stability. We provide the full Pytorch-style pseudocode of this training algorithm in Appendix B.1. In comparison to the block-parallel forms described Section 2, both GLA and linear attention can leverage tensor cores for inter-chunk computations. For intra-chunk computations, while linear attention models can directly leverage tensor cores, GLA layers need to rely on another level of chunking due to numerical instability. As a middle ground between linear attention and GLA, we consider removing α_t or β_t for further improving efficiency, keeping a partially fine-grained gating scheme. As we will show later in the experiments, removing β_t only leads to a very minor difference in performance while offering significant runtime improvements.

3.4 GLA-Transformer

We incorporate the multi-head design from softmax-attention into GLA layers. Given H heads, the recurrent form of a multi-head GLA layer is given by (for $h \in [1, H]$),

$$\begin{aligned} \mathbf{S}_t^h &= \mathbf{G}_t^h \odot \mathbf{S}_{t-1}^h + \mathbf{K}_t^{h\top} \mathbf{V}_t^h \in \mathbb{R}^{d'_k \times d'_v}, \\ \mathbf{O}_t^h &= \mathbf{Q}_t^{h\top} \mathbf{S}_t^h \in \mathbb{R}^{1 \times d'_v}, \\ \mathbf{O}'_t &= \text{concat}(\text{LN}(\mathbf{O}_t^1), \dots, \text{LN}(\mathbf{O}_t^H)) \in \mathbb{R}^{1 \times d_v}, \\ \mathbf{R}_t &= \text{Swish}(\mathbf{X}_t \mathbf{W}_r + \mathbf{b}_r) \in \mathbb{R}^{1 \times d_v}, \\ \mathbf{Y}_t &= (\mathbf{R}_t \odot \mathbf{O}'_t) \mathbf{W}_O \in \mathbb{R}^{1 \times d}. \end{aligned}$$

Here $d'_k = d_k/H, d'_v = d_v/H$ are per-head key/value dimensions, and LayerNorm is applied after the output of each head individually following RetNet (Sun et al., 2023). The output projection and output gating operate on the concatenation of head outputs.

We then build up a Transformer-like model by interleaving multi-head GLA layers with feed-forward networks (FFN). Concretely, given layer l ’s contextualized representation $\mathbf{X}^{(l)}$, we obtain $\mathbf{X}^{(l+1)}$ via

$$\mathbf{Y}^{(l)} = \text{GLA}(\text{LN}(\mathbf{X}^{(l)})) + \mathbf{X}^{(l)}, \quad \mathbf{X}^{(l+1)} = \text{SwiGLU}(\text{LN}(\mathbf{Y}^{(l)})),$$

where we use the SwiGLU FFN layer following Touvron et al. (2023),

$$\text{SwiGLU}(\mathbf{Z}) = (\text{Swish}(\mathbf{Z}\mathbf{W}_1) \odot \mathbf{Z}\mathbf{W}_2)\mathbf{W}_3.$$

¹³See Appendix B.1 for the derivation.

¹⁴This design maximizes the usage of half-precision matmuls and is motivated by the intuition that tokens inside the same sub-chunk are more important than the ones outside; thus, $\mathbf{P}_{[i][i]}$ requires higher precision to compute than $\mathbf{P}_{[i][j]}$ for $i < j$.

Parameter allocation. As presented, our GLA layer employs three additional weight matrices (i.e., $\mathbf{W}_\alpha, \mathbf{W}_\beta, \mathbf{W}_r$) compared to an ordinary softmax-attention layer, which only has $\mathbf{W}_K, \mathbf{W}_Q, \mathbf{W}_V, \mathbf{W}_O$. Thus a direct parameterization of GLA with ($d_k = d_v = d$) would require $7d^2$ parameters. We explore three strategies for reducing the number of parameters. First, even though our algorithm theoretically allows for different β_t 's, we found in preliminary experiments that \mathbf{W}_β contributes very marginally to the final performance (as we show in our ablation study). Hence, we remove it (i.e., $\beta_t = 1$) to save parameters and speed up training. Second, we use a low-rank parameterization to replace \mathbf{W}_α ,

$$\boldsymbol{\alpha} = \sigma(\mathbf{X}\mathbf{W}_\alpha^1\mathbf{W}_\alpha^2 + \mathbf{b}_\alpha)/\tau \in \mathbb{R}^{L \times d_k},$$

where $\mathbf{W}_\alpha^1 \in \mathbb{R}^{d \times 16}$, $\mathbf{W}_\alpha^2 \in \mathbb{R}^{16 \times d_k}$. Finally, we set $d_k = \frac{d}{2}$ and $d_v = d$ and use full-rank parameterizations for $(\mathbf{W}_Q, \mathbf{W}_K, \mathbf{W}_V, \mathbf{W}_O, \mathbf{W}_r)$. As a result, the number of parameters for $\boldsymbol{\alpha}$ and $\boldsymbol{\beta}$ is negligible, and one GLA layer collectively needs (roughly) $4d^2$ parameters, allowing for fair comparison against an ordinary softmax attention layer. We also follow the parameter allocation of LLaMA (Touvron et al., 2023) where the hidden size of SwiGLU is set $\frac{4}{3}d$ so that the parameter size of the FFN layer is $8d^2$.

4 Empirical Study

We test our gated linear attention Transformer (GLA-Transformer) on moderate-scale language modeling. Our experiments are primarily aimed at studying whether the GLA-Transformer can perform competitively against (1) strong Transformer baselines with modern architectural/training recipes and (2) recent architectures that have also been proposed as efficient (i.e., subquadratic) alternatives to Transformers.

4.1 Experimental Setup

Baselines. We evaluate the GLA-Transformer against three baselines: Transformer⁺⁺ (Touvron et al., 2023), RetNet (Sun et al., 2023), and Mamba (Gu & Dao, 2023). Transformer⁺⁺ is the LLaMA architecture with Rotary Positional Embeddings (Su et al., 2021), SWiGLU (Shazeer, 2020) and RMSNorm (Zhang & Sennrich, 2019); we also use SwiGLU in the RetNet to replace its original FFN. For Mamba, we use the open-source code.¹⁵ For fair comparison our baselines are trained for the exact same number of tokens with the same optimization settings.

Dataset. We use the SlimPajama dataset¹⁶ and tokenize it using the Mistral tokenizer.¹⁷ The original dataset contains 627B tokens; we use a 100B subset for pre-training our models.

Training details. We train all models from scratch at two scales: 340M¹⁸ and 1.3B. All models are trained with the AdamW (Loshchilov & Hutter, 2018) using a maximum learning rate of 3e-4. The 340M models are trained on 15B tokens with a batch size of 0.5M tokens, while the 1.3B models are trained on 100B tokens with a batch size of 2M tokens. We use a cosine learning rate schedule with a warmup of 0.5B/1B tokens for the 340M/1.3B settings respectively. The initial and final learning rates are 3e-5. We use a weight decay of 0.01, and gradient clipping of 1.0.

Evaluation. In addition to perplexity (ppl) on Wikitext (Wiki.), we consider a wide range of downstream tasks covering common-sense reasoning and question-answering as was used in Gu & Dao (2023): LAMBADA (LMB.; Paperno et al., 2016), PiQA (Bisk et al., 2020), HellaSwag (Hella.; Zellers et al., 2019), Wino-Grande (Wino.; Sakaguchi et al., 2021), ARC-easy (ARC-e) and ARC-challenge (Arc-c) (Clark et al., 2018). In Appendix C, we also include results on additional tasks: CoQA (Reddy et al., 2019), SciQA (Auer et al., 2023), OpenbookQA (Mihaylov et al., 2018), BoolQA (Clark et al., 2019). We report perplexity (ppl) on WikiText and LAMBADA, accuracy normalized by length on HellaSwag, ARC-challenge and OpenbookQA, and accuracy on the other tasks. All the evaluations are conducted using the LM evaluation harness (Gao et al., 2021).

¹⁵<https://github.com/state-spaces/mamba>

¹⁶<https://huggingface.co/datasets/cerebras/SlimPajama-627B>

¹⁷<https://huggingface.co/mistralai/Mistral-7B-v0.1>

¹⁸The RetNet and Mamba baselines have 350M parameters in this setting due to slight differences parameterizaton.

Model	Wiki. ppl ↓	LMB. ppl ↓	LMB. acc ↑	PIQA acc ↑	Hella. acc_norm ↑	Wino. acc ↑	ARC-e acc ↑	ARC-c acc_norm ↑	Avg.
<i>0-shot, 15B training tokens</i>									
Transformer ⁺⁺ (340M)	28.39	42.69	31.0	63.3	34.0	50.4	44.5	24.2	41.2
RetNet (350M)	32.33	49.19	28.6	63.5	33.5	52.5	44.5	23.4	41.0
Mamba (350M)	28.39	39.66	30.6	65.0	35.4	50.1	46.3	23.6	41.8
GLA-Transformer (340M)	28.65	43.35	30.3	64.8	34.5	51.4	45.1	22.7	41.5
<i>0-shot, 100B training tokens</i>									
Transformer ⁺⁺ (1.3B)	16.85	13.44	48.9	70.8	49.6	53.6	56.0	26.5	50.9
RetNet (1.3B)	18.64	17.27	43.3	70.0	47.3	52.5	54.8	25.6	48.9
Mamba (1.3B)	17.06	13.89	46.2	72.2	40.1	54.1	59.0	28.2	50.0
GLA-Transformer (1.3B)	17.29	13.65	46.6	71.2	49.4	53.1	56.6	26.8	50.6
<i>5-shot, 100B training tokens</i>									
Transformer ⁺⁺ (1.3B)	-	16.80	42.9	70.2	50.3	53.8	60.5	28.7	51.1
RetNet (1.3B)	-	23.27	37.3	69.8	47.5	51.1	58.5	27.4	48.6
Mamba (1.3B)	-	23.00	37.4	71.4	51.2	54.1	60.1	30.4	50.8
GLA-Transformer (1.3B)	-	20.84	38.3	70.8	49.9	53.8	62.9	27.8	50.6

Table 1: GLA-Transformer results against Transformer⁺⁺ (Touvron et al., 2023), RetNet (Sun et al., 2023), and Mamba (Gu & Dao, 2023). All models are trained on the same subset of the SlimPajama dataset with the Mistral tokenizer. The 340M/1.3B models are trained for 15B/100B tokens respectively. For the 1.3B models we show both zero- and five-shot performance. We report the main results on the same set of tasks reported by Gu & Dao (2023). See Appendix C for results on other benchmarks. The last column shows the average over all benchmarks that use (normalized) accuracy as the metric.

4.2 Results

Main results. Our main results are shown in Table 1. Compared to RetNet which uses a data-independent decay rate, the GLA-Transformer with data-dependent gates shows improved results on all tasks, indicating the importance of fine-grained gates. Both GLA-Transformer and Mamba show comparable performance as Transformer⁺⁺, in both the zero- and five-shot settings.

Ablation on GLA layer parameterization. The GLA parameterization (i.e., $d_k = d/2, d_v = d, \beta_t = 1, \text{num_head} = 4$) used in the main experiments were found by the following ablation study, where we conducted a set of small-scale experiments by training variants of 340M GLAs for 7B tokens, and used the average perplexity of the last 200 training steps for quick evaluation.

The results are shown in Table 2. Our base version uses both gates (i.e., α, β). We draw several key observations: 1) β is not necessary and removing it leads to a marginal improvements, 2) α is crucial and removing it leads to worse performance, 3) having a smaller head dimension (where we increase num_head from 4 to 8) hurts performance. However, we observed a diminishing return when using a larger head dimension, e.g. reducing the num_head from 4 to 1.

Training ppl.		
α	β	
✓	✓	14.86
✓	✗	14.73
✗	✓	15.15
✗	✗	23.21
small head dim.		15.29
large head dim.		14.61

Table 2: Ablation study results.

Speed analysis. We benchmark runtime speed using a setting that resembles our pretraining setting in the main experiments: BFloat16 input, batch size 32, model dimension 1024. We first compare our Triton-based implementation of GLA (with both α, β for a fair comparison) against the CUDA-based implementation of Mao (2022), which uses the recurrent form and materializes hidden states of all steps into HBM. As we can see in Table 3, our chunk-parallel based implementation leads to significant speedup and memory savings. Their implementation encounters the memory issue under moderate head dimension and sentence length, while ours can afford a much larger head dimension (in practice, we can scale up the

Length	Head dim.	Speed-up	Memory
1k	64	3.8x	0.26x
1k	128	2.8x	0.13x
2k	64	2.3x	0.26x
2k	128	-	OOM

Table 3: Benchmark speed-up and memory footprint against the CUDA implementation of Mao (2022), which uses the recurrent form and materializes the hidden states into HBM. OOM indicates out of memory in Mao (2022)’s implementation.

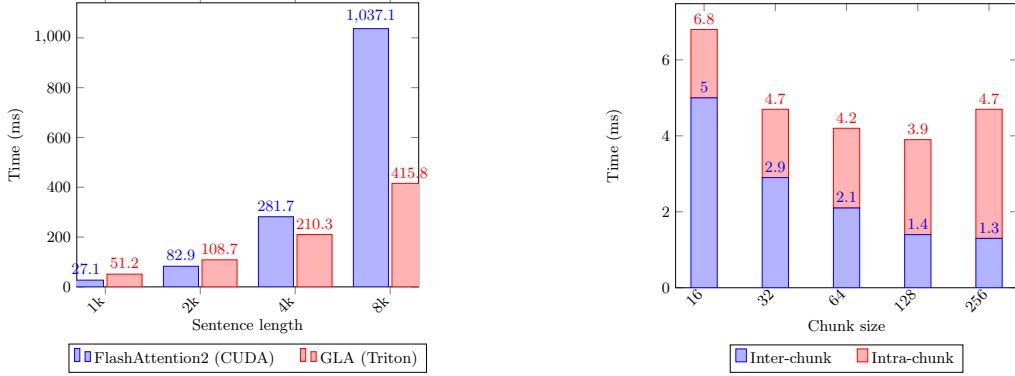


Figure 2: (Left) Running time (forward+backward pass) comparison between CUDA-optimized FlashAttention-2 (DAO, 2023) and our Triton-implementation of GLA. (Right) The running time ratio (forward pass) of intra- and inter-chunk computation when varying chunk size.

head dimension up to the model dimension d). We next compare our Triton-based implementation against CUDA-optimized FlashAttention-2 (DAO, 2023), in particular FlashAttention with 16 heads versus GLA (without β) with 4 heads. Figure 2 (left) shows the results. GLA performs comparably to FlashAttention-2 under the regular 2048 sentence length setting, while outperforming FlashAttention-2 beyond 4096 due to the subquadratic complexity. In Figure 2 (right) we vary the chunk size and show the ratio of intra- and inter-chunk computations. Inter-chunk computation is mainly bottlenecked by the HBM I/O cost, while intra-chunk computation is mainly bottlenecked by FLOPs. The best chunk size that balances between HBM I/O cost and FLOPs is 128.

5 Related Work

Linear RNNs/SSMs/Transformers. Traditional RNNs are difficult to scale due to the nonlinear dependencies between the hidden states and expensive matmul-based sequential hidden state updates. Linear RNNs/State-Space Models (SSMs)/Transformers eliminate nonlinear dependencies, making training parallelizable along the temporal dimension (Martin & Cundy, 2018; Gu et al., 2022a; Smith et al., 2023). Such models have been the focus of much recent work as a competitive sub-quadratic alternative to the Transformer architecture (Gu & Dao, 2023; Qin et al., 2023b;a; Sun et al., 2023; Wang et al., 2022). We next discuss two ongoing directions to improve these linear RNN models: using data-dependent decay rates and expanding hidden state dimension.

Data-dependent decay rates have always been regarded important for RNNs. Initially introduced by Gers et al. (2000), forget gates have become a crucial component for practical sequence modeling with RNNs, and are believed to be key to the empirical success of LSTMs (van der Westhuizen & Lasenby, 2018). Typical forget gate values depend on both the previous hidden state and the current input. However Martin & Cundy (2018) suggest that forget gate values should depend solely on the current inputs to enable parallel training. This simple strategy has been shown effective in moderate-scale experiments conducted by HGRN (Qin et al., 2023a). RWKV-v6 (Peng et al., 2023) and Mamba (Gu & Dao, 2023) also use data-dependent decay rates

that are reminiscent of forget gates. In the context of linear Transformers, Peng et al. (2021) employ a coarse-grained position-wise forget gate, while Mao (2022) and Pramanik et al. (2023) use a more fine-grained forget gate with outer-product-based parameterizations. We follow the latter setting and address the efficiency issues encountered by these works. Our parallel form closely resembles the parallel form for data-dependent gated linear attention concurrent work (GateLoop; Katsch, 2023). The main difference is that our parallel form is more general since gates can be applied in both \mathbf{K} and \mathbf{V} dimensions, while only the gate for the \mathbf{K} dimension is applied in Katsch (2023). Moreover, in practice Katsch (2023) used the recurrent form, as opposed to the parallel form, in the actual implementation via parallel scan (potentially due to the numerical issue discussed in section 3), while we rely on our chunk-wise block-parallel form.

RNNs rely on fixed-dimensional hidden states to encode their entire history. The hidden state dimension serves as a proxy for memory capacity and thus significantly influences their expressive power. Linear Transformers expand the hidden dimension via the outer-product parameterization, as discussed §2.1. Linear SSMs on the other hand expand their hidden dimension via a single-input-single-output (SISO) strategy. Without data-dependent SSM parameters, this can be done efficiently during training via the Fast Fourier Transform (FFT). However, with data-dependent SSM parameters, FFT-based training is not possible, and thus Gu & Dao (2023) implement a custom CUDA kernel for training a selective state-space model using the parallel scan algorithm (Smith et al., 2023). To fit all the hidden states into SRAM, they can only afford an expansion rate up to 16. In contrast our hardware-aware training algorithm provides an alternative, efficient approach for expanding the hidden dimension to a wider range by employing the structural properties of the Kronecker/outer product.

Chunk-level parallelism in sequence modeling. The chunk-wise parallel form of linear Transformers resembles the two-stage parallel prefix sum (or parallel scan) algorithm (Blelloch, 1990), which also combines chunk-wise parallel computations with inter-chunk communication. It also resembles sequence parallelism used for accelerating attention-based Transformers (Li et al., 2023b), which has recently received much attention for long-sequence modeling (Liu et al., 2023; Li et al., 2023a; Brandon et al., 2023). Sequence-level parallelism also constitutes the main improvement of FlashAttention-2 (Dao, 2023) over FlashAttention-1 (Dao et al., 2022). The main differences between these works are that 1) the chunk-level parallel form of linear Transformer needs only a single pass due to the linear complexity, while the sequence parallelism in Transformers needs L/C passes (i.e., left-to-right scan of key/value blocks for each query block) due to the inherent quadratic complexity, and 2) the order of matrix multiplications is different.

6 Conclusion

We propose an efficient algorithm for training linear attention Transformers with data-dependent gating mechanisms. Our algorithm makes it possible to balance FLOPs against parallelism, while still allowing for the use of half-precision matmuls which can take advantage of tensor core units on modern GPUs. Experiments on language modeling at moderate scale demonstrate that gated linear attention Transformers can perform respectably compared to strong Transformer and state-space model baselines.

Acknowledgments

This work was supported by MIT-IBM Watson AI. We thank Yutao Sun, Zhen Qin, Li Dong, Xinyu Yang, Jiacheng You, and Huanqi Cao for helpful discussions.

References

Sören Auer, Dante A. C. Barone, Cassiano Bartz, Eduardo G. Cortes, Mohamad Yaser Jaradeh, Oliver Karras, Manolis Koubarakis, Dmitry Mouromtsev, Dmitrii Pliukhin, Daniil Radyush, Ivan Shilin, Markus Stocker, and Eleni Tsalapati. The sciqa scientific question answering benchmark for scholarly knowledge. *Scientific Reports*, 13(1):7240, May 2023. ISSN 2045-2322. doi: 10.1038/s41598-023-33607-z. URL <https://doi.org/10.1038/s41598-023-33607-z>.

Jimmy Ba, Geoffrey E Hinton, Volodymyr Mnih, Joel Z Leibo, and Catalin Ionescu. Using fast weights to attend to the recent past. *Advances in neural information processing systems*, 29, 2016.

Yonatan Bisk, Rowan Zellers, Jianfeng Gao, Yejin Choi, et al. Piqa: Reasoning about physical commonsense in natural language. In *Proceedings of the AAAI conference on artificial intelligence*, volume 34, pp. 7432–7439, 2020.

Guy E. Blelloch. Prefix sums and their applications. 1990. URL <https://api.semanticscholar.org/CorpusID:60459178>.

William Brandon, Aniruddha Nrusimha, Kevin Qian, Zachary Ankner, Tian Jin, Zhiye Song, and Jonathan Ragan-Kelley. Striped attention: Faster ring attention for causal transformers. *ArXiv*, abs/2311.09431, 2023. URL <https://api.semanticscholar.org/CorpusID:265220849>.

Kyunghyun Cho, Bart Van Merriënboer, Caglar Gulcehre, Dzmitry Bahdanau, Fethi Bougares, Holger Schwenk, and Yoshua Bengio. Learning phrase representations using rnn encoder-decoder for statistical machine translation. *arXiv preprint arXiv:1406.1078*, 2014.

Jack Choquette, Edward Lee, Ronny Krashinsky, Vishnu Balan, and Brucek Khailany. 3.2 the a100 datacenter gpu and ampere architecture. In *2021 IEEE International Solid-State Circuits Conference (ISSCC)*, volume 64, pp. 48–50, 2021. doi: 10.1109/ISSCC42613.2021.9365803.

Krzysztof Choromanski, Valerii Likhoshesterov, David Dohan, Xingyou Song, Andreea Gane, Tamas Sarlos, Peter Hawkins, Jared Davis, Afroz Mohiuddin, Lukasz Kaiser, et al. Rethinking attention with performers. *arXiv preprint arXiv:2009.14794*, 2020.

Christopher Clark, Kenton Lee, Ming-Wei Chang, Tom Kwiatkowski, Michael Collins, and Kristina Toutanova. Boolq: Exploring the surprising difficulty of natural yes/no questions. *arXiv preprint arXiv:1905.10044*, 2019.

Peter Clark, Isaac Cowhey, Oren Etzioni, Tushar Khot, Ashish Sabharwal, Carissa Schoenick, and Oyvind Tafjord. Think you have solved question answering? try arc, the ai2 reasoning challenge. *arXiv preprint arXiv:1803.05457*, 2018.

Abdul Dakkak, Cheng Li, Jinjun Xiong, Isaac Gelado, and Wen-Mei W. Hwu. Accelerating reduction and scan using tensor core units. In Rudolf Eigenmann, Chen Ding, and Sally A. McKee (eds.), *Proceedings of the ACM International Conference on Supercomputing, ICS 2019, Phoenix, AZ, USA, June 26-28, 2019*, pp. 46–57. ACM, 2019. doi: 10.1145/3330345.3331057. URL <https://doi.org/10.1145/3330345.3331057>.

Tri Dao. Flashattention-2: Faster attention with better parallelism and work partitioning. *CoRR*, abs/2307.08691, 2023. doi: 10.48550/ARXIV.2307.08691. URL <https://doi.org/10.48550/arXiv.2307.08691>.

Tri Dao, Daniel Y. Fu, Stefano Ermon, Atri Rudra, and Christopher Ré. Flashattention: Fast and memory-efficient exact attention with io-awareness. In *NeurIPS*, 2022. URL http://papers.nips.cc/paper_files/paper/2022/hash/67d57c32e20fd0a7a302cb81d36e40d5-Abstract-Conference.html.

Daniel Y. Fu, Hermann Kumbong, Eric Nguyen, and Christopher Ré. Flashfftconv: Efficient convolutions for long sequences with tensor cores. *CoRR*, abs/2311.05908, 2023. doi: 10.48550/ARXIV.2311.05908. URL <https://doi.org/10.48550/arXiv.2311.05908>.

Leo Gao, Jonathan Tow, Stella Biderman, Sid Black, Anthony DiPofi, Charles Foster, Laurence Golding, Jeffrey Hsu, Kyle McDonell, Niklas Muennighoff, Jason Phang, Laria Reynolds, Eric Tang, Anish Thite, Ben Wang, Kevin Wang, and Andy Zou. A framework for few-shot language model evaluation, September 2021. URL <https://doi.org/10.5281/zenodo.5371628>.

Felix A. Gers, Jürgen Schmidhuber, and Fred A. Cummins. Learning to forget: Continual prediction with LSTM. *Neural Comput.*, 12(10):2451–2471, 2000. doi: 10.1162/089976600300015015. URL <https://doi.org/10.1162/089976600300015015>.

Albert Gu and Tri Dao. Mamba: Linear-time sequence modeling with selective state spaces. 2023. URL <https://api.semanticscholar.org/CorpusID:265551773>.

Albert Gu, Karan Goel, and Christopher Ré. Efficiently modeling long sequences with structured state spaces. In *The Tenth International Conference on Learning Representations, ICLR 2022, Virtual Event, April 25-29, 2022*. OpenReview.net, 2022a. URL <https://openreview.net/forum?id=uYLFoz1vlAC>.

Albert Gu, Karan Goel, and Christopher Ré. Efficiently modeling long sequences with structured state spaces, 2022b.

Franz A. Heinsen. Efficient parallelization of an ubiquitous sequential computation. 2023. URL <https://api.semanticscholar.org/CorpusID:265149785>.

Geoffrey E Hinton and David C Plaut. Using fast weights to deblur old memories. In *Proceedings of the ninth annual conference of the Cognitive Science Society*, pp. 177–186, 1987.

Sepp Hochreiter and Jürgen Schmidhuber. Long short-term memory. *Neural Computation*, 9(8):1735–1780, 1997.

Weizhe Hua, Zihang Dai, Hanxiao Liu, and Quoc V. Le. Transformer quality in linear time. In Kamalika Chaudhuri, Stefanie Jegelka, Le Song, Csaba Szepesvári, Gang Niu, and Sivan Sabato (eds.), *International Conference on Machine Learning, ICML 2022, 17-23 July 2022, Baltimore, Maryland, USA*, volume 162 of *Proceedings of Machine Learning Research*, pp. 9099–9117. PMLR, 2022. URL <https://proceedings.mlr.press/v162/hua22a.html>.

Kazuki Irie, Imanol Schlag, Róbert Csordás, and Jürgen Schmidhuber. Going beyond linear transformers with recurrent fast weight programmers. *Advances in Neural Information Processing Systems*, 34:7703–7717, 2021.

Jungo Kasai, Hao Peng, Yizhe Zhang, Dani Yogatama, Gabriel Ilharco, Nikolaos Pappas, Yi Mao, Weizhu Chen, and Noah A. Smith. Finetuning pretrained transformers into rnns. In Marie-Francine Moens, Xuanjing Huang, Lucia Specia, and Scott Wen-tau Yih (eds.), *Proceedings of the 2021 Conference on Empirical Methods in Natural Language Processing, EMNLP 2021, Virtual Event / Punta Cana, Dominican Republic, 7-11 November, 2021*, pp. 10630–10643. Association for Computational Linguistics, 2021a. doi: 10.18653/V1/2021.EMNLP-MAIN.830. URL <https://doi.org/10.18653/v1/2021.emnlp-main.830>.

Jungo Kasai, Hao Peng, Yizhe Zhang, Dani Yogatama, Gabriel Ilharco, Nikolaos Pappas, Yi Mao, Weizhu Chen, and Noah A. Smith. Finetuning pretrained transformers into RNNs. In Marie-Francine Moens, Xuanjing Huang, Lucia Specia, and Scott Wen-tau Yih (eds.), *Proceedings of the 2021 Conference on Empirical Methods in Natural Language Processing*, pp. 10630–10643, Online and Punta Cana, Dominican Republic, November 2021b. Association for Computational Linguistics. doi: 10.18653/v1/2021.emnlp-main.830. URL <https://aclanthology.org/2021.emnlp-main.830>.

Angelos Katharopoulos, Apoorv Vyas, Nikolaos Pappas, and François Fleuret. Transformers are rnns: Fast autoregressive transformers with linear attention. In *International conference on machine learning*, pp. 5156–5165. PMLR, 2020.

Tobias Katsch. Gateloop: Fully data-controlled linear recurrence for sequence modeling. *ArXiv*, abs/2311.01927, 2023. URL <https://api.semanticscholar.org/CorpusID:265018962>.

Bin-Rui Li, Shenggan Cheng, and James Lin. tcfft: Accelerating half-precision FFT through tensor cores. *CoRR*, abs/2104.11471, 2021. URL <https://arxiv.org/abs/2104.11471>.

Dacheng Li, Rulin Shao, Anze Xie, Eric P. Xing, Joseph E. Gonzalez, Ion Stoica, Xuezhe Ma, and Hao Zhang. Lightseq: Sequence level parallelism for distributed training of long context transformers. *ArXiv*, abs/2310.03294, 2023a. URL <https://api.semanticscholar.org/CorpusID:263671659>.

Shenggui Li, Fuzhao Xue, Chaitanya Baranwal, Yongbin Li, and Yang You. Sequence parallelism: Long sequence training from system perspective. In Anna Rogers, Jordan Boyd-Graber, and Naoaki Okazaki (eds.), *Proceedings of the 61st Annual Meeting of the Association for Computational Linguistics (Volume 1: Long Papers)*, pp. 2391–2404, Toronto, Canada, July 2023b. Association for Computational Linguistics. doi: 10.18653/v1/2023.acl-long.134. URL <https://aclanthology.org/2023.acl-long.134>.

Lucas D. Lingle. Transformer-vq: Linear-time transformers via vector quantization. *CoRR*, abs/2309.16354, 2023. doi: 10.48550/ARXIV.2309.16354. URL <https://doi.org/10.48550/arXiv.2309.16354>.

Hao Liu, Matei Zaharia, and Pieter Abbeel. Ring attention with blockwise transformers for near-infinite context. *ArXiv*, abs/2310.01889, 2023. URL <https://api.semanticscholar.org/CorpusID:263608461>.

Ilya Loshchilov and Frank Hutter. Fixing weight decay regularization in adam. 2018.

Huanru Henry Mao. Fine-tuning pre-trained transformers into decaying fast weights. In *Proceedings of the 2022 Conference on Empirical Methods in Natural Language Processing*, pp. 10236–10242, Abu Dhabi, United Arab Emirates, December 2022. Association for Computational Linguistics. doi: 10.18653/v1/2022.emnlp-main.697. URL <https://aclanthology.org/2022.emnlp-main.697>.

Eric Martin and Chris Cundy. Parallelizing linear recurrent neural nets over sequence length. In *6th International Conference on Learning Representations, ICLR 2018, Vancouver, BC, Canada, April 30 - May 3, 2018, Conference Track Proceedings*. OpenReview.net, 2018. URL <https://openreview.net/forum?id=HyUNwulC->.

Harsh Mehta, Ankit Gupta, Ashok Cutkosky, and Behnam Neyshabur. Long range language modeling via gated state spaces. In *The Eleventh International Conference on Learning Representations, ICLR 2023, Kigali, Rwanda, May 1-5, 2023*. OpenReview.net, 2023. URL <https://openreview.net/pdf?id=5MkYIYCbva>.

Todor Mihaylov, Peter Clark, Tushar Khot, and Ashish Sabharwal. Can a suit of armor conduct electricity? a new dataset for open book question answering. *arXiv preprint arXiv:1809.02789*, 2018.

Denis Paperno, Germán Kruszewski, Angeliki Lazaridou, Quan Ngoc Pham, Raffaella Bernardi, Sandro Pezzelle, Marco Baroni, Gemma Boleda, and Raquel Fernández. The lambada dataset: Word prediction requiring a broad discourse context. *arXiv preprint arXiv:1606.06031*, 2016.

Bo Peng, Eric Alcaide, Quentin Anthony, Alon Albalak, Samuel Arcadinho, Huanqi Cao, Xin Cheng, Michael Chung, Matteo Grella, Kranthi Kiran G. V., Xuzheng He, Haowen Hou, Przemyslaw Kazienko, Jan Kocon, Jiaming Kong, Bartłomiej Koptyra, Hayden Lau, Krishna Sri Ipsit Mantri, Ferdinand Mom, Atsushi Saito, Xiangru Tang, Bolun Wang, Johan S. Wind, Stanislaw Wozniak, Ruichong Zhang, Zhenyuan Zhang, Qihang Zhao, Peng Zhou, Jian Zhu, and Rui-Jie Zhu. RWKV: reinventing rnns for the transformer era. *CoRR*, abs/2305.13048, 2023. doi: 10.48550/ARXIV.2305.13048. URL <https://doi.org/10.48550/arXiv.2305.13048>.

Hao Peng, Nikolaos Pappas, Dani Yogatama, Roy Schwartz, Noah A Smith, and Lingpeng Kong. Random feature attention. *arXiv preprint arXiv:2103.02143*, 2021.

Louis Pisha and Lukasz Ligowski. Accelerating non-power-of-2 size fourier transforms with GPU tensor cores. In *35th IEEE International Parallel and Distributed Processing Symposium, IPDPS 2021, Portland, OR, USA, May 17-21, 2021*, pp. 507–516. IEEE, 2021. doi: 10.1109/IPDPS49936.2021.00059. URL <https://doi.org/10.1109/IPDPS49936.2021.00059>.

Subhojeet Pramanik, Esraa Elelimy, Marlos C. Machado, and Adam White. Recurrent linear transformers. *CoRR*, abs/2310.15719, 2023. doi: 10.48550/ARXIV.2310.15719. URL <https://doi.org/10.48550/arXiv.2310.15719>.

Zhen Qin, Xiaodong Han, Weixuan Sun, Dongxu Li, Lingpeng Kong, Nick Barnes, and Yiran Zhong. The devil in linear transformer. *arXiv preprint arXiv:2210.10340*, 2022.

Zhen Qin, Dong Li, Weigao Sun, Weixuan Sun, Xuyang Shen, Xiaodong Han, Yunshen Wei, Baohong Lv, Fei Yuan, Xiao Luo, et al. Scaling transnromer to 175 billion parameters. *arXiv preprint arXiv:2307.14995*, 2023a.

Zhen Qin, Songlin Yang, and Yiran Zhong. Hierarchically gated recurrent neural network for sequence modeling. *CoRR*, abs/2311.04823, 2023b. doi: 10.48550/ARXIV.2311.04823. URL <https://doi.org/10.48550/arXiv.2311.04823>.

Prajit Ramachandran, Barret Zoph, and Quoc V. Le. Swish: a self-gated activation function. *arXiv: Neural and Evolutionary Computing*, 2017. URL <https://api.semanticscholar.org/CorpusID:196158220>.

Siva Reddy, Danqi Chen, and Christopher D Manning. Coqa: A conversational question answering challenge. *Transactions of the Association for Computational Linguistics*, 7:249–266, 2019.

Keisuke Sakaguchi, Ronan Le Bras, Chandra Bhagavatula, and Yejin Choi. Winogrande: An adversarial winograd schema challenge at scale. *Communications of the ACM*, 64(9):99–106, 2021.

Imanol Schlag, Kazuki Irie, and Jürgen Schmidhuber. Linear transformers are secretly fast weight programmers. In Marina Meila and Tong Zhang (eds.), *Proceedings of the 38th International Conference on Machine Learning, ICML 2021, 18-24 July 2021, Virtual Event*, volume 139 of *Proceedings of Machine Learning Research*, pp. 9355–9366. PMLR, 2021. URL <http://proceedings.mlr.press/v139/schlag21a.html>.

Jürgen Schmidhuber. Learning to control fast-weight memories: An alternative to dynamic recurrent networks. *Neural Computation*, 4(1):131–139, 1992.

Noam Shazeer. Glu variants improve transformer. *arXiv preprint arXiv:2002.05202*, 2020.

Jimmy T. H. Smith, Andrew Warrington, and Scott W. Linderman. Simplified state space layers for sequence modeling. In *The Eleventh International Conference on Learning Representations, ICLR 2023, Kigali, Rwanda, May 1-5, 2023*. OpenReview.net, 2023. URL <https://openreview.net/pdf?id=Ai8Hw3AXqks>.

Jianlin Su, Yu Lu, Shengfeng Pan, Bo Wen, and Yunfeng Liu. Roformer: Enhanced transformer with rotary position embedding. *CoRR*, abs/2104.09864, 2021. URL <https://arxiv.org/abs/2104.09864>.

Yutao Sun, Li Dong, Shaohan Huang, Shuming Ma, Yuqing Xia, Jilong Xue, Jianyong Wang, and Furu Wei. Retentive network: A successor to transformer for large language models. *arXiv preprint arXiv:2307.08621*, 2023.

Philippe Tillet, Hsiang-Tsung Kung, and David D. Cox. Triton: an intermediate language and compiler for tiled neural network computations. In Tim Mattson, Abdullah Muzahid, and Armando Solar-Lezama (eds.), *Proceedings of the 3rd ACM SIGPLAN International Workshop on Machine Learning and Programming Languages, MAPL@PLDI 2019, Phoenix, AZ, USA, June 22, 2019*, pp. 10–19. ACM, 2019. doi: 10.1145/3315508.3329973. URL <https://doi.org/10.1145/3315508.3329973>.

Hugo Touvron, Thibaut Lavril, Gautier Izacard, Xavier Martinet, Marie-Anne Lachaux, Timothée Lacroix, Baptiste Rozière, Naman Goyal, Eric Hambro, Faisal Azhar, et al. Llama: Open and efficient foundation language models. *arXiv preprint arXiv:2302.13971*, 2023.

Jos van der Westhuizen and Joan Lasenby. The unreasonable effectiveness of the forget gate. *CoRR*, abs/1804.04849, 2018. URL <http://arxiv.org/abs/1804.04849>.

Ashish Vaswani, Noam Shazeer, Niki Parmar, Jakob Uszkoreit, Llion Jones, Aidan N Gomez, Łukasz Kaiser, and Illia Polosukhin. Attention is all you need. *Advances in neural information processing systems*, 30, 2017.

Junxiong Wang, Jing Nathan Yan, Albert Gu, and Alexander M. Rush. Pretraining without attention. *CoRR*, abs/2212.10544, 2022. doi: 10.48550/ARXIV.2212.10544. URL <https://doi.org/10.48550/arXiv.2212.10544>.

Jing Nathan Yan, Jiatao Gu, and Alexander M. Rush. Diffusion models without attention. 2023. URL <https://api.semanticscholar.org/CorpusID:265506646>.

Rowan Zellers, Ari Holtzman, Yonatan Bisk, Ali Farhadi, and Yejin Choi. Hellaswag: Can a machine really finish your sentence? *arXiv preprint arXiv:1905.07830*, 2019.

Biao Zhang and Rico Sennrich. Root mean square layer normalization. *Advances in Neural Information Processing Systems*, 32, 2019.

Appendix

A Extended Background on Hardware Considerations

(Our presentation here roughly follows those of the backgrounds presented in section 2.1 of [Dao et al. \(2022\)](#) and section 2.2 of [Fu et al. \(2023\)](#).) GPUs have a large number of threads to execute an operation (called a kernel). Threads are organized into thread blocks, and each thread block is scheduled to run on a streaming multiprocessor (SM). For example, there are 108 SMs on an A100. GPU operations can be either memory-bound or compute-bound, depending on whether the dominant factor in the total runtime is memory access or actual computational time. Examples of memory-bound operations include element-wise operations such as additions, while examples of compute-bound operations include dense matrix multiplications (matmuls).

The running time of memory-bound operations is determined by the total number of memory accesses required and the memory bandwidth in different parts of the memory hierarchy. Specifically, a GPU has larger (but slower) high bandwidth memory (HBM) that is shared across all streaming multiprocessors (SM), and smaller (but faster) shared RAM (SRAM) that is shared between threads within an SM. (Each thread has its own register.) For example an A100 has 40-80GB of HBM with bandwidth of 1.5-2.0TB/s and 40MB of on-chip SRAM with bandwidth of around 19TB/s. Optimal utilization of SRAM to reduce HBM I/O cost can therefore lead to significant speed ups; for example, the attention mechanism is memory-bound and benefits significantly from tiling and kernel fusion, as demonstrated in FlashAttention-1 ([Dao et al., 2022](#)).

The running time of compute-bound operations, on the other hand, is determined by the total number of floating-point operations (FLOPs) required and the processing unit's floating-point operations per second (FLOP/s). Half-precision (FP16/BF16) matmuls benefit significantly from *tensor cores*, which are specialized processing units on modern GPUs that have been optimized specifically for matmuls. For example, tensor core matmuls achieve speeds up to 312 TFLOP/s on an A100 GPU, whereas other operations in FP32 format reach only 19.5 TFLOP/s ([Choquette et al., 2021](#)). Thus, half-precision matmuls on an A100 can be roughly 16 times faster, and recent works such as FlashAttention-2 ([Dao, 2023](#)) and FlashConvFFT ([Fu et al., 2023](#)) aim to minimize FLOPs in non-half-precision matmul operations as much as possible.

B Gated linear attention: More details

B.1 Psudocode for two-level chunking

```
1 def gated_linear_attention(Q, K, V, log_alpha, log_beta, C, c):
2     # Args:
3     #   Q/K : Query, Key vectors
4     #       (Batch Size: B, Number of Head: H, Input Sequence Length: L, Head Size: D_K)
5     #   V: Value vector
6     #       (Batch Size: B, Number of Head: H, Input Sequence Length: L, Head Size: D_V)
7     #   log_alpha: log score of forget gate values in the K dimension
8     #       (Batch Size: B, Number of Head: H, Input Sequence Length: L, Head Size: D_K)
9     #   log_beta: log score of forget gate values in the V dimension
10    #       (Batch Size: B, Number of Head: H, Input Sequence Length: L, Head Size: D_V)
11    #   C: chunk size of the first-level chunking
12    #   c: chunk size of the secondary-level chunking
13    # Returns:
14    #   O: output vector
15    #       (Batch Size: B, Number of Head: H, Input Sequence Length: L, Head Size: D_V)
16
17    B, H, L, D_K = Q.shape
18    D_V = V.shape[-1]
19
20    # compute cumulative product of forget gates in log-space
21    A = log_alpha.cumsum(-2)
22    B = log_beta.cumsum(-2)
23    KV = torch.zeros(B, H, L // C, D_K, D_V)
24
25    ## perform reduction for each chunk i in parallel
26    for i in range(L // C):
27        k = K[:, :, i*C:(i+1)*C]
```

```

28     a = A[:, :, i*C:(i+1)*C, :]
29     b = B[:, :, i*C:(i+1)*C, :]
30     k = k * (a[:, :, -1, None, :] - a).exp()
31     v = v * (b[:, :, -1, None, :] - b).exp()
32     KV[:, :, i] = k.transpose(-1, -2) @ v
33
34     ## recurrent update of chunk-level hidden state
35     S = torch.zeros(B, H, L // C, D_K, D_V)
36     for i in range(1, L//C):
37         decay_A = (A[:, :, (i+1)*C-1, :] - A[:, :, i*C-1, :]).exp()
38         decay_B = (B[:, :, (i+1)*C-1, :] - B[:, :, i*C-1, :]).exp()
39         decay = decay_A.unsqueeze(-1) * decay_B.unsqueeze(-2)
40         S[:, :, i] = S[:, :, i-1] * decay + KV[:, :, i]
41
42     # output of inter-chunk computation
43     O1 = torch.zeros(B, H, L, D_V)
44     # output of intra-chunk computation
45     O2 = torch.zeros(B, H, L, D_V)
46
47     ## inter-chunk computation for each chunk i in parallel
48     for i in range(L // C):
49         a = A[:, :, i*C:(i+1)*C, :]
50         b = B[:, :, i*C:(i+1)*C, :]
51         q = Q[:, :, i*C:(i+1)*C, :]
52         q = q * (a - a[:, :, 0, None, :]).exp()
53         o = q @ S[:, :, i, :, :]
54         o = o * (b - b[:, :, 0, None, :]).exp()
55         O1[:, :, (i*C):(i+1)*C, :] = o
56
57     # causal mask for self-attention of each subchunk
58     mask = torch.triu(torch.ones(c, c), diagonal=1)
59
60     ## blockwise intra-chunk computation for each chunk i in parallel
61     for i in range(L//C):
62         for j in range(0, C//c):
63             o = torch.zeros(B, H, c, D_V)
64             q = Q[:, :, i*C+j*c:i*C+(j+1)*c, :]
65             a_q = A[:, :, i*C+j*c:i*C+(j+1)*c, :]
66             b_q = B[:, :, i*C+j*c:i*C+(j+1)*c, :]
67             a_normalizer = a[:, :, 0, :]
68             b_normalizer = b[:, :, 0, :]
69             q = q * (a_q - a_normalizer.unsqueeze(-2)).exp()
70
71         ## inter-sub-chunk computation
72         for k in range(0, j):
73             k = K[:, :, i*C+k*c:i*C+(k+1)*c, :]
74             v = V[:, :, i*C+k*c:i*C+(k+1)*c, :]
75             a_kv = A[:, :, i*C+k*c:i*C+(k+1)*c, :]
76             b_kv = B[:, :, i*C+k*c:i*C+(k+1)*c, :]
77             k = k * (a_normalizer.unsqueeze(-2) - a_kv).exp()
78             v = v * (b_normalizer.unsqueeze(-2) - b_kv).exp()
79             qk = q @ k.transpose(-1, -2)
80             o += (qk @ v) * (b_q - b_normalizer.unsqueeze(-2)).exp()
81
82     ## intra-sub-chunk computation
83     # caveat: numerically unstable, only for demonstration.
84     k = K[:, :, i*C+k*c:i*C+(j+1)*c, :]
85     v = V[:, :, i*C+k*c:i*C+(j+1)*c, :]
86     k = k * (a_normalizer.unsqueeze(-2) - a_q).exp()
87     v = v * (b_normalizer.unsqueeze(-2) - b_q).exp()
88     qk = (q @ k.transpose(-1, -2)).masked_fill_(mask, 0)
89     o += (qk @ v) * (b_q - b_normalizer.unsqueeze(-2)).exp()
90     O2[:, :, i*C+j*c:i*C+(j+1)*c, :] = o
91
92     O = O1 + O2
93

```

Listing 1: Pytorch-like code snippet for Gated Linear Attention.

B.2 Useful Lemmas

Lemma 1. For $\mathbf{x}, \mathbf{y}, \mathbf{z} \in \mathbb{R}^d$,

$$\langle \mathbf{x}, \mathbf{y} \odot \mathbf{z} \rangle = \langle \mathbf{x}, \mathbf{z} \odot \mathbf{y} \rangle$$

Proof.

$$\begin{aligned} \langle \mathbf{x}, \mathbf{y} \odot \mathbf{z} \rangle &= \sum_{i=1}^d (\mathbf{x}_i \mathbf{y}_i) \mathbf{z}_i \\ &= \sum_{i=1}^d \mathbf{x}_i (\mathbf{y}_i \mathbf{z}_i) \\ &= \langle \mathbf{x}, \mathbf{z} \odot \mathbf{y} \rangle \end{aligned}$$

□

Lemma 2. For $\mathbf{A} \in \mathbb{R}^{m \times n}, \mathbf{B} \in \mathbb{R}^{k \times n}, \mathbf{c} \in \mathbb{R}^n$, then,

$$\mathbf{AB}^\top = (\mathbf{A} \odot \mathbf{c}) \left(\frac{\mathbf{B}}{\mathbf{c}} \right)^\top$$

Proof.

$$\begin{aligned} (\mathbf{AB}^\top)_{ij} &= \sum_{l=1}^n \mathbf{A}_{il} \mathbf{B}_{jl} \\ &= \sum_{l=1}^n (\mathbf{A}_{il} \mathbf{c}_l) \frac{\mathbf{B}_{jl}}{\mathbf{c}_l} \\ &= \sum_{l=1}^n (\mathbf{A} \odot \mathbf{c})_{il} \left(\frac{\mathbf{B}}{\mathbf{c}} \right)_{jl} \\ &= \left((\mathbf{A} \odot \mathbf{c}) \left(\frac{\mathbf{B}}{\mathbf{c}} \right)^\top \right)_{ij} \end{aligned}$$

□

Lemma 3. For $\mathbf{A} \in \mathbb{R}^{m \times n}, \mathbf{B} \in \mathbb{R}^{n \times k}, \mathbf{c} \in \mathbb{R}^k$, then,

$$(\mathbf{AB}) \odot \mathbf{c} = \mathbf{A}(\mathbf{B} \odot \mathbf{c})$$

Proof.

$$\begin{aligned} ((\mathbf{AB}) \odot \mathbf{c})_{ij} &= \left(\sum_{l=1}^n \mathbf{A}_{il} \mathbf{B}_{lj} \right) \mathbf{c}_j \\ &= \sum_{l=1}^n \mathbf{A}_{il} (\mathbf{B}_{lj} \mathbf{c}_j) \\ &= \sum_{l=1}^n \mathbf{A}_{il} (\mathbf{B} \odot \mathbf{c})_{lj} \\ &= (\mathbf{A}(\mathbf{B} \odot \mathbf{c}))_{ij} \end{aligned}$$

□

Lemma 4. For $\mathbf{x}, \mathbf{y} \in \mathbb{R}^{1 \times m}, \mathbf{z} \in \mathbb{R}^{1 \times n}, \mathbf{A} \in \mathbb{R}^{m \times n}$, then,

$$\mathbf{x} \left((\mathbf{y}^\top \mathbf{z}) \odot \mathbf{A} \right) = ((\mathbf{x} \odot \mathbf{y}) \mathbf{A}) \odot \mathbf{z} \in \mathbb{R}^{1 \times n}$$

Proof.

$$\begin{aligned} \left(\mathbf{x} \left((\mathbf{y}^\top \mathbf{z}) \odot \mathbf{A} \right) \right)_j &= \sum_k \mathbf{x}_k \left(\left((\mathbf{y}^\top \mathbf{z}) \odot \mathbf{A} \right) \right)_{kj} \\ &= \sum_k (\mathbf{x}_k \mathbf{A}_{kj} \mathbf{y}_k \mathbf{z}_j) \\ &= \mathbf{z}_j \sum_k (\mathbf{x}_k \mathbf{y}_k) \mathbf{A}_{kj} \\ &= \mathbf{z}_j ((\mathbf{x} \odot \mathbf{y}) \mathbf{A})_j \\ &= (((\mathbf{x} \odot \mathbf{y}) \mathbf{A}) \odot \mathbf{z})_j \end{aligned}$$

□

B.3 Parallel form

Based on Eq.12 and the mixed product property of Kronecker/outer product, we have

$$\left(\prod_{j=i+1}^t \mathbf{G}_j \right) \odot (\mathbf{K}_i^\top \mathbf{V}_i) = \left(\left(\frac{\mathbf{A}_t}{\mathbf{A}_i} \right)^\top \left(\frac{\mathbf{B}_t}{\mathbf{B}_i} \right) \right) \odot (\mathbf{K}_i^\top \mathbf{V}_i) \quad (18)$$

$$= \left(\frac{\mathbf{A}_t}{\mathbf{A}_i} \odot \mathbf{K}_i \right)^\top \left(\frac{\mathbf{B}_t}{\mathbf{B}_i} \odot \mathbf{V}_i \right) \quad (19)$$

Put it together, we have,

$$\mathbf{O}_t = \mathbf{Q}_t \mathbf{S}_t = \mathbf{Q}_t \sum_{i=1}^t \left(\left(\prod_{j=i+1}^t \mathbf{G}_j \right) \odot (\mathbf{K}_i^\top \mathbf{V}_i) \right) \quad (20)$$

$$= \mathbf{Q}_t \sum_{i=1}^t \left(\frac{\mathbf{A}_t}{\mathbf{A}_i} \odot \mathbf{K}_i \right)^\top \left(\frac{\mathbf{B}_t}{\mathbf{B}_i} \odot \mathbf{V}_i \right) \quad (21)$$

$$= \sum_{i=1}^t \left(\mathbf{Q}_t \left(\frac{\mathbf{A}_t}{\mathbf{A}_i} \odot \mathbf{K}_i \right)^\top \right) \left(\frac{\mathbf{B}_t}{\mathbf{B}_i} \odot \mathbf{V}_i \right) \quad (22)$$

$$= \sum_{i=1}^t \underbrace{\left\langle \mathbf{Q}_t, \frac{\mathbf{K}_i}{\mathbf{A}_i} \odot \mathbf{A}_t \right\rangle}_{\mathbb{R}^{1 \times 1}} \underbrace{\left(\frac{\mathbf{V}_i}{\mathbf{B}_i} \odot \mathbf{B}_t \right)}_{\mathbb{R}^{1 \times d_v}} \quad (23)$$

$$= \sum_{i=1}^t \left(\left\langle \mathbf{Q}_t \odot \mathbf{A}_t, \frac{\mathbf{K}_i}{\mathbf{A}_i} \right\rangle \frac{\mathbf{V}_i}{\mathbf{B}_i} \right) \odot \mathbf{B}_t \quad (24)$$

$$= \sum_{i=1}^t \left((\mathbf{Q}_t \odot \mathbf{A}_t) \left(\frac{\mathbf{K}_i}{\mathbf{A}_i} \right)^\top \left(\frac{\mathbf{V}_i}{\mathbf{B}_i} \right) \right) \odot \mathbf{B}_t \in \mathbb{R}^{1 \times d_v} \quad (25)$$

Eq. 22 is by linearity and associative property of matrix multiplication, Eq. 24 is by Lemma 1. The above form has the following equivalent parallel form similar to the parallel form of linear/softmax attention.

$$\tilde{\mathbf{Q}} = \mathbf{Q} \odot \mathbf{A} \quad \tilde{\mathbf{K}} = \mathbf{K} / \mathbf{A} \quad \tilde{\mathbf{V}} = \mathbf{V} / \mathbf{B} \quad (26)$$

$$\tilde{\mathbf{O}} = (\tilde{\mathbf{Q}} \tilde{\mathbf{K}}^\top \odot \mathbf{M}) \tilde{\mathbf{V}} \quad \mathbf{O} = \tilde{\mathbf{O}} \odot \mathbf{B} \quad (27)$$

where $\mathbf{Q}, \mathbf{K}, \mathbf{A} \in \mathbb{R}^{L \times d_k}, \mathbf{V}, \mathbf{B} \in \mathbb{R}^{L \times d_v}, \mathbf{M} \in \mathbb{R}^{L \times L}$ denotes the causal mask.

Numerical stability. For the parallel form, we can define two matrix multiplication operations $\circledast_{\mathbf{A}}, \boxtimes_{\mathbf{B}}$ as follows:

$$\mathbf{P}_{ij} = (\mathbf{Q} \circledast_{\mathbf{A}} \mathbf{K}^{\top})_{ij} = \begin{cases} \sum_k \exp(\log \mathbf{A}_{ik} - \log \mathbf{A}_{jk}) \mathbf{Q}_{ik} \mathbf{K}_{jk}, & i \geq j \\ 0, & i < j \end{cases} \quad (28)$$

$$\mathbf{O}_{ij} = (\mathbf{P} \boxtimes_{\mathbf{B}} \mathbf{V})_{ij} = \sum_{k \leq i} \exp(\log \mathbf{B}_{ij} - \log \mathbf{B}_{kj}) \mathbf{P}_{ik} \mathbf{V}_{kj} \quad (29)$$

This could be considered as *generalized matrix multiplication* with a customized semiring.¹⁹ Developing a specialized CUDA kernel based on this new semiring could be an interesting direction to directly utilize the parallel form for training.

B.4 Chunkwise parallel form

$$\mathbf{S}_{[i+1]} = \left(\prod_{j=iC+1}^{(i+1)C} \mathbf{G}_j \right) \odot \mathbf{S}_{[i]} + \sum_{j=iC+1}^{(i+1)C} \left(\prod_{k=j+1}^{(i+1)C} \mathbf{G}_k \right) \odot (\mathbf{K}_j^{\top} \mathbf{V}_j) \quad (30)$$

$$= \left(\left(\frac{\mathbf{A}_{(i+1)C}}{\mathbf{A}_{iC}} \right)^{\top} \left(\frac{\mathbf{B}_{(i+1)C}}{\mathbf{B}_{iC}} \right) \right) \odot \mathbf{S}_{[i]} + \underbrace{\sum_{j=iC+1}^{(i+1)C} \left(\frac{\mathbf{A}_{(i+1)C}}{\mathbf{A}_j} \odot \mathbf{K}_j \right)^{\top} \left(\frac{\mathbf{B}_{(i+1)C}}{\mathbf{B}_j} \odot \mathbf{V}_j \right)}_{(\mathbf{A}'_{[i+1]} \odot \mathbf{K}_{[i+1]})^{\top} (\mathbf{B}'_{[i+1]} \odot \mathbf{V}_{[i+1]})} \quad (31)$$

where $(\mathbf{A}'_{[i+1]})_j = \frac{\mathbf{A}_{(i+1)C}}{\mathbf{A}_{iC+j}}$ for $j \in \{1, \dots, C\}$ and likewise for $\mathbf{B}'_{[i+1]}$.

$$\mathbf{S}_{iC+j} = \left(\left(\prod_{k=i}^j \mathbf{G}_{iC+j} \right) \odot \mathbf{S}_{iC} \right) + \sum_{k=1}^j \left(\left(\prod_{m=k}^j \mathbf{G}_{iC+m} \right) \odot (\mathbf{K}_{iC+k}^{\top} \mathbf{V}_{iC+k}) \right) \quad (32)$$

Then,

$$\mathbf{O}_{iC+j} = \mathbf{Q}_{iC+j} \mathbf{S}_{iC+j} = \underbrace{\mathbf{Q}_{iC+j} \left(\left(\prod_{k=i}^j \mathbf{G}_{iC+j} \right) \odot \mathbf{S}_{iC} \right)}_{(1)} + \underbrace{\mathbf{Q}_{iC+j} \left(\sum_{k=1}^j \left(\left(\prod_{m=k}^j \mathbf{G}_{iC+m} \right) \odot (\mathbf{K}_{iC+k}^{\top} \mathbf{V}_{iC+k}) \right) \right)}_{(2)} \quad (33)$$

(2) can be computed similarly to Eq. 27.

For (1),

$$(1) = \mathbf{Q}_{iC+j} \left(\left(\left(\frac{\mathbf{A}^{iC+j}}{\mathbf{A}^{iC}} \right)^{\top} \frac{\mathbf{B}^{iC+j}}{\mathbf{B}^{iC}} \right) \odot \mathbf{S}_{[i]} \right) \quad (34)$$

$$= \left((\mathbf{Q}_{iC+j} \odot \frac{\mathbf{A}^{iC+j}}{\mathbf{A}^{iC}}) \mathbf{S}_{[i]} \right) \odot \frac{\mathbf{B}^{iC+j}}{\mathbf{B}^{iC}} \quad (35)$$

$$= \left(\left((\mathbf{Q}_{[i]})_j \odot (\mathbf{A}_{[i]}^{\dagger})_j \right) \mathbf{S}_{[i]} \right) \odot \left(\mathbf{B}_{[i]}^{\dagger} \right)_j \quad (36)$$

where Eq. 35 is by Lemma 4. Putting it together, we have

$$\mathbf{O}_{[i+1]} = \underbrace{\left((\mathbf{Q}_{[i+1]} \odot \mathbf{A}_{[i+1]}^{\dagger}) \mathbf{S}_{[i]} \right) \odot \mathbf{B}_{[i+1]}^{\dagger}}_{\text{previous-chunk}} + \underbrace{(\tilde{\mathbf{Q}}_{[i+1]} \tilde{\mathbf{K}}_{[i+1]}^{\top} \odot \mathbf{M}) \tilde{\mathbf{V}}_{[i+1]}}_{\text{intra-chunk}}, \quad (37)$$

¹⁹See <https://github.com/harvardnlp/genbmm> for more examples.

B.5 Secondary-level chunking

Continuing from Eq.27, we have

$$\mathbf{P}_{[i],[j]} = (\mathbf{Q}_{[i]} \odot \mathbf{A}_{[i]})(\frac{\mathbf{K}_{[j]}}{\mathbf{A}_{[j]}})^\top \quad (38)$$

$$= (\mathbf{Q}_{[i]} \odot \frac{\mathbf{A}_{[i]}}{\mathbf{A}_{iC}})(\mathbf{K}_{[j]} \odot \frac{\mathbf{A}_{iC}}{\mathbf{A}_{[j]}})^\top \quad (39)$$

$$= (\mathbf{Q}_{[i]} \odot \frac{\mathbf{A}_{[i]}}{\mathbf{A}_{iC}})(\mathbf{K}_{[j]} \odot \frac{\mathbf{A}_{(j+1)C}}{\mathbf{A}_{[j]}} \odot \frac{\mathbf{A}_{iC}}{\mathbf{A}_{(j+1)C}})^\top \quad (40)$$

$$= (\mathbf{Q}_{[i]} \odot \mathbf{A}_{[i]}^\dagger)(\mathbf{K}_{[j]} \odot \mathbf{A}'_{[j]} \odot \frac{\mathbf{A}_{iC}}{\mathbf{A}_{(j+1)C}})^\top \quad (41)$$

where Eq.39 is by Lemma 2. We slightly abuse the notation of \odot to have broadcast-ed elementwise product. Similarly,

$$\mathbf{O}_{[i],[j]} = (\mathbf{P}_{[i][j]} \frac{\mathbf{V}_{[j]}}{\mathbf{B}_{[j]}}) \odot \mathbf{B}_{[i]} \quad (42)$$

$$= (\mathbf{P}_{[i][j]} \frac{\mathbf{V}_{[j]}}{\mathbf{B}_{[j]}}) \odot \mathbf{B}_{[i]} \quad (43)$$

$$= (\mathbf{P}_{[i][j]} \frac{\mathbf{V}_{[j]}}{\mathbf{B}_{[j]}} \odot \mathbf{B}_{(j+1)C}) \odot \frac{\mathbf{B}_{[i]}}{\mathbf{B}_{(j+1)C}} \quad (44)$$

$$= \left(\mathbf{P}_{[i][j]} \left(\mathbf{V}_{[j]} \odot \frac{\mathbf{B}_{(j+1)C}}{\mathbf{B}_{[j]}} \right) \right) \odot \left(\frac{\mathbf{B}_{[i]}}{\mathbf{B}_{iC}} \odot \frac{\mathbf{B}_{iC}}{\mathbf{B}_{(j+1)C}} \right) \quad (45)$$

$$= \left(\mathbf{P}_{[i][j]} \left(\mathbf{V}_{[j]} \odot \mathbf{B}'_{[j]} \right) \right) \odot \left(\mathbf{B}_{[i]}^\dagger \odot \frac{\mathbf{B}_{iC}}{\mathbf{B}_{(j+1)C}} \right) \quad (46)$$

where Eq. 44 is based on Lemma 2 and Eq. 45 is based on Lemma 3.

C Additional Results

Model	Wiki. ppl ↓	LMB. ppl ↓	PIQA. acc ↑	Hella. acc_norm ↑	Wino. acc ↑	ARC-e acc ↑	ARC-c acc_norm ↑	CoQA acc ↑	OBQA acc_norm ↑	SciQA acc ↑	BoolQA acc ↑	Avg.
<i>0-shot</i>												
Transformer ⁺⁺ 340M	28.39	42.69	31.0	63.3	34.0	50.4	44.5	24.2	66.0	28.4	73.8	60.9
RetNet 350M	32.33	49.19	28.6	63.5	33.5	52.5	44.5	23.4	63	28.4	73.1	60.0
Mamba 350M	28.39	39.66	30.6	65.0	35.4	50.1	46.3	23.6	71.0	28.4	73.7	52.6
GLA-Transformer 340M	28.65	43.35	30.3	64.8	34.5	51.4	45.1	22.7	70.0	29.2	73.2	58.7
<i>θ-shot</i>												
Transformer ⁺⁺ 1.3B	16.85	13.44	48.9	70.8	49.6	53.6	56.0	26.5	75.0	29.8	83.6	52.3
RetNet 1.3B	18.64	17.27	43.3	70.0	47.3	52.5	54.8	25.6	70.0	31.4	82.3	57.1
Mamba 1.3B	17.06	13.89	46.2	72.2	40.1	54.1	59.0	28.2	74.0	33.0	83.1	59.1
GLA-Transformer 1.3B	17.29	13.65	46.6	71.2	49.4	53.1	56.6	26.8	71.0	32.4	83.0	57.9
<i>5-shot</i>												
Transformer ⁺⁺ 1.3B	-	16.80	42.9	70.2	50.3	53.8	60.5	28.7	75.0	33.8	90.7	46.0
RetNet 1.3B	-	23.27	37.3	69.8	47.5	51.1	58.5	27.4	72.0	31.8	87.5	45.3
Mamba 1.3B	-	23.00	31.4	71.4	51.2	54.1	60.1	30.4	79.0	33.8	88.5	47.7
GLA-Transformer 1.3B	-	20.84	38.31	70.8	49.9	53.8	62.9	27.8	75.0	33.0	89.1	49.6

Table 4: Extended zero- and five-shot performance results. All models are trained on the same subset of SlimPajama dataset with Mistral tokenizer. The 350M/1.3B models are trained for 15B/100B tokens respectively. The last column shows the average of all accuracies.